Supplemental Material

For

The preparation of the MF_6^- (M = As, Sb) salts of 1,4-benzoquinodal bridged bis-1,3,2-dithiazolylium utilizing the cycloaddition and oxidative dehydrogenation chemistry of $SNSMF_6$ and observation of a hybrid semiquinoidal-thiazyl radical cation by EPR

Andreas Decken,[a] Aaron Mailman,[a] and Jack Passmore*[a]

Table of contents: **page 1-4**

[a] Department of Chemistry, University of New Brunswick, Fredericton, Canada, NB, E3B 5A3; [*] Tel: 5064544981; E-mail: passmore@unb.ca

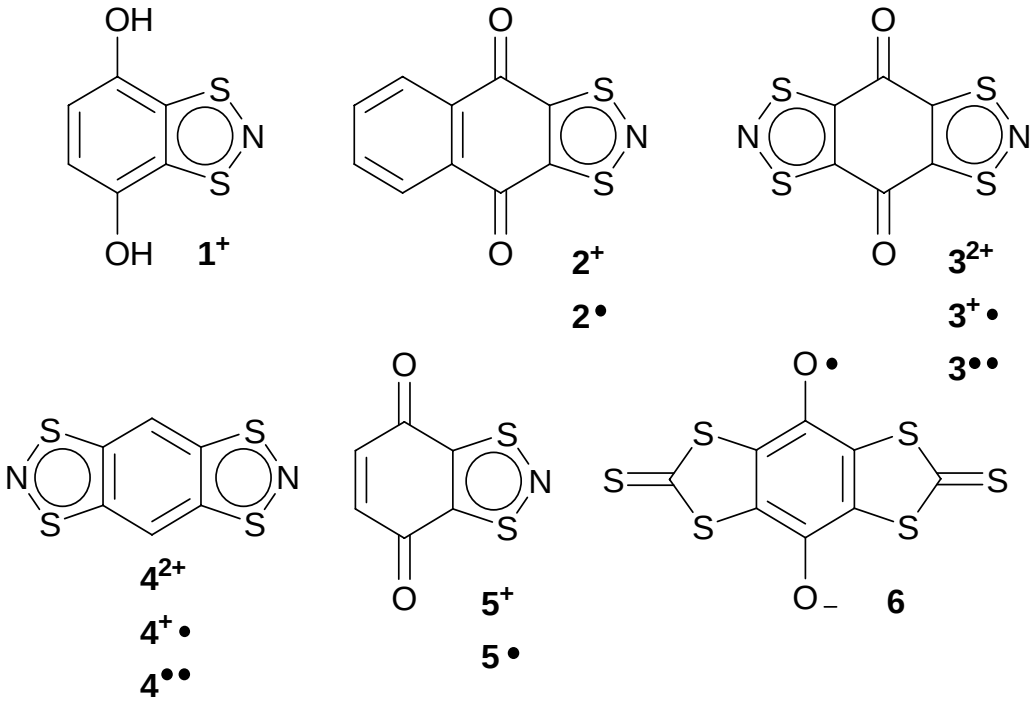

Chart 1: Molecules of Interest

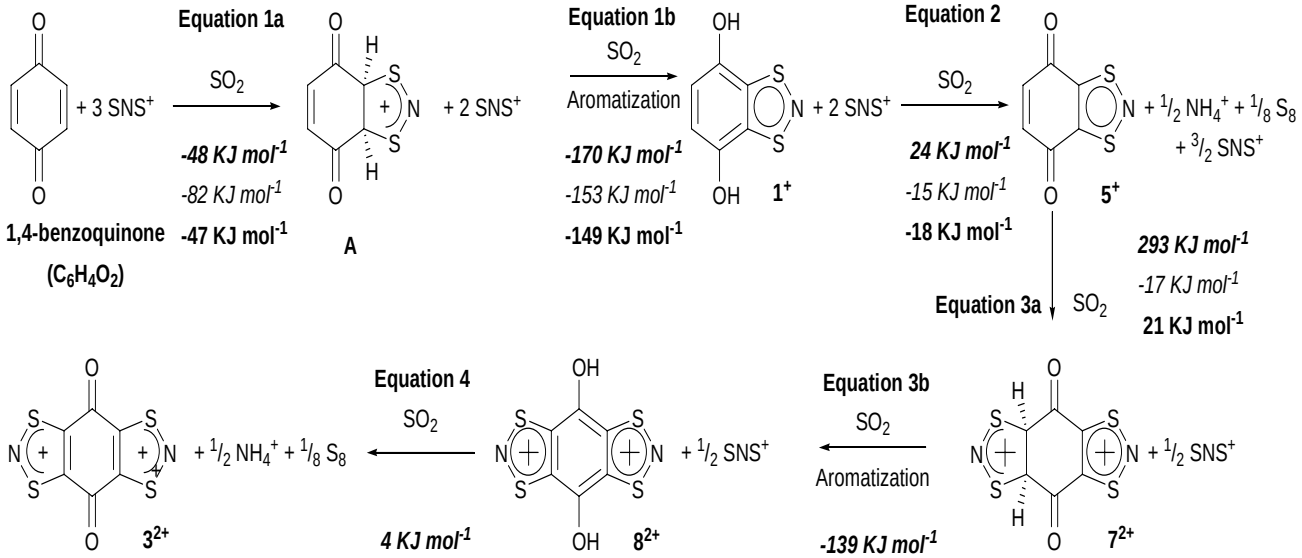

Calculated in gas phase
B3LYP/6-311++G(d,p)
Enthalpy (△H)

Calculated in SO_2
Solution PBEO/6-311G(d)
Enthalpy (△H)
Gibbs free energy (△G)

Scheme 1

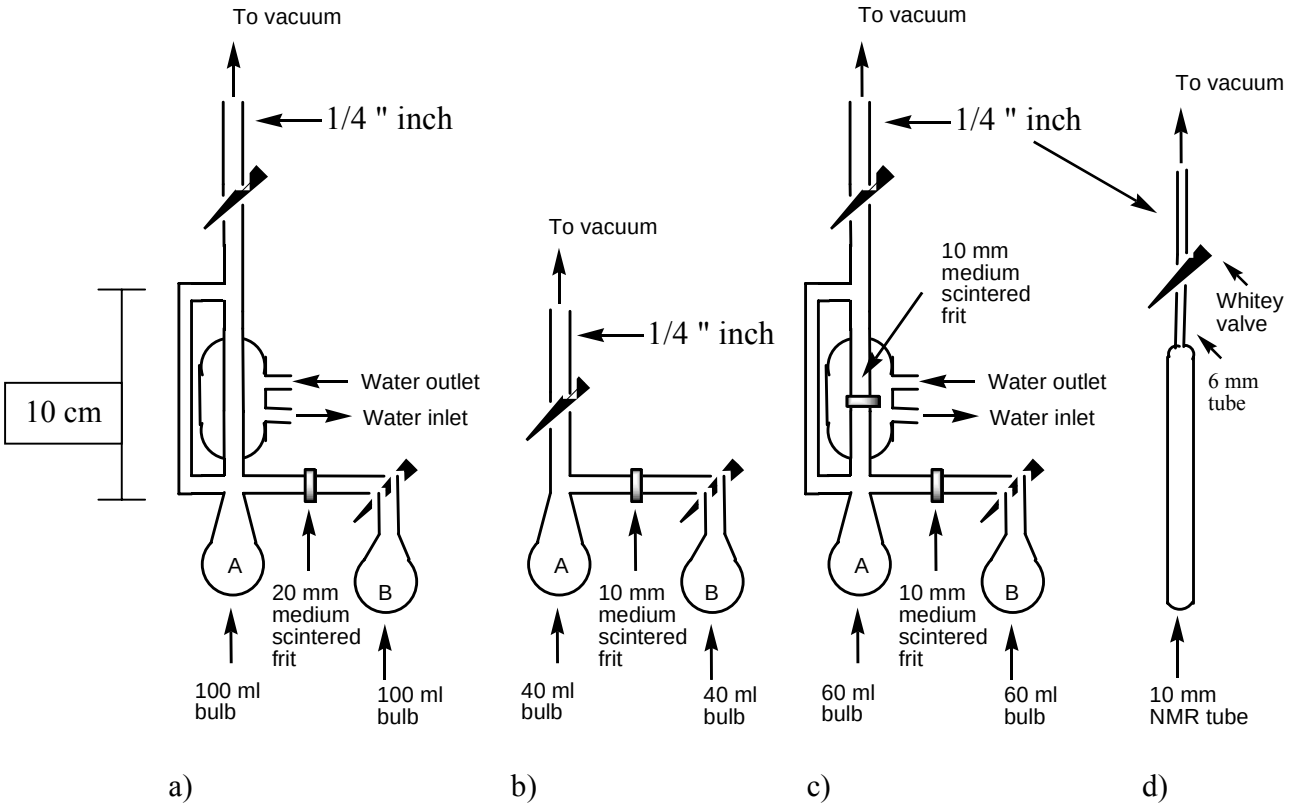

Figure S1: One piece Pyrex vessels used in Experimental section.

S1: Experimental Section:

1.1 Materials: $SNSMF_6$ (M = As, Sb) were prepared and purified according to literature procedures. Ferrocene (Cp_2Fe, Aldrich, 98%) and 1,4-benzoquinone (Aldrich, 98%) were purified by vacuum sublimation prior to use. Arsenic pentaflouride (AsF_5, Ozark-Mahoney, 98%) was used as received or prepared from AsF_3 according to literature procedure[1]. CsI (Strem, 98 %) was used as received. Sulfur dioxide (SO_2, Liquid Air, 99.9998% was stored over CaH_2 for at least 24 hrs and freshly distilled prior to use (*Caution!* SO_2 is a condensable gas with a high vapour pressure (~3.25 atm at 20^{o}C) which should be handled in well ventilated fumehood, leather gloves, face shield, blast shield, carefully built pyrex vessel). Acetonitrile (CH_3CN, HPLC grade) and dichloromethane (CH_2Cl_2, HPLC grade) were dried over refluxing CaH_2 for 24 hrs and distilled onto fresh CaH_2 under nitrogen atmosphere. Acetonitrile was degassed by three freeze-pump-thaw cycles and freshly distilled *in vacuo* prior to use.

1.2 General Procedures. Pyrex vessels of three types (Figure S1a-c) were employed throughout unless otherwise stated: Type A, incorporating a water cooled reflux condenser and two bulbs (100 ml) separated by a 20 mm medium frit and closed by two Rotoflo (6 HK) Teflon in glass valves (See Figure S1a) Type B, incorporating two bulbs (40 ml) separated by a 10 mm medium scintered frit and closed by two J. Young (POR/10/RA) Teflon in glass valves (See Figure S1b) with a Teflon coated stir bar in bulb B. Type C, incorporating a 10 mm medium scintered frit centered in a water cooled condenser with a pressure equilizing side-arm with two 60 ml bulbs separated by a second 10 mm medium scintered frit and two Rotoflo (6 HK) Teflon in glass valves (See

Figure S1c). One piece 10 mm (o.d.) NMR tubes with ¼ inch (6 mm, o.d.) Pyrex tube were connected to stainless steel Whitey® valves (1KS4) by Swagelok® compression fittings, using Teflon back and front ferrules. The Whitey® valves were attached directly to the vacuum line by ¼ inch Monel tubing (See Figure S1d). The NMR tubes were cooled with liquid N_2 and flame sealed at the ¼ inch (6 mm) Pyrex tube.

Solids were manipulated under a dry N_2 or Argon atmosphere in an MBraun drybox ($O_2 \leq 0.1$ ppm and $H_2O \leq 0.1$ ppm). Techniques and apparatus for carrying out reactions in SO_2 in a closed greaseless Monel vacuum line, such that volatile materials can be transferred quantitatively, have been described elsewhere.[2]

FT-IR spectra were recorded on a Thermo Nicolet NEXUS 470 FT-IR (32 scans, resolution 2 cm^{-1}) as Nujol mulls between CsI or KBr plates.

Dispersive Raman microscopy at 298 K of samples contained in sealed melting point tubes were recorded on a Renishaw inVia RE 08 microscope with CCD detector (diode laser operating at 785 nm, 10 mW laser power at the source, ~ 1 mW at the sample, 4 cm^{-1} resolution, 20 scans with cosmic ray removal).

Electron paramagnetic resonance (EPR) solution spectra were obtained on an X-band Magnettech MS200 high sensitivity X-band (9.3 - 9.55 GHz) spectrometer. Microwave frequencies were measured with an XL Microwave, model 5200 frequency counter.

NMR spectra were recorded on a Varian 400 NMR spectrometer in 10 mm NMR tubes that were flame sealed. The ^{1}H-NMR (399.945 MHz, 25 ^{o}C) were recorded with a minimum of 20 transients and were externally referenced to TMS (^{1}H). Both the coupled and decoupled ^{13}C-NMR (100.58 MHz, 25 ^{o}C) were recorded with a minimum of 2000 transients and a standard line broadening of 4 used to reduce signal to noise and were externally referenced to TMS (^{13}C). The ^{14}N-NMR (28.901 MHz, 25 ^{o}C) were recorded at 25 ^{o}C with a minimum of 500 transients and a standard line broadening of 40-48 applied to reduce signal to noise and were externally referenced to neat nitromethane (^{14}N). The ^{19}F-NMR (370 MHz, 25 ^{o}C) were recorded with a minimum of 20 transients and were externally referenced to $CFCl_3$ (^{19}F) in SO_2. ^{13}C-NMR spectra obtained in CD_3CN were recorded with a minimum of 10000 transients and referenced internally to the solvent (CH_3-***C***N, δ 118.26 ppm).[3] Elemental analyses were carried out by Galbraith Laboratories, Inc., Knoxville, TN, USA.

Calculated (B3LYP/6-311++G(d,p)) structures and NMR tensors with correlation method (See Table S2 below):

All geometries were optimized and found to be true minima by vibration analysis at the B3LYP/6-311++G(d,p) level of theory using the Gaussian 03W suite of programmes.[4] The geometries of $\mathbf{1}^{+}$ (C_2v), $\mathbf{3}^{2+}$ (C_2), $\mathbf{5}^{+}$ (C_2v), $\mathbf{5}^{\bullet}$ (C_2v), $\mathbf{7}^{2+}$ (C_1), $\mathbf{8}^{2+}$ (C_1) and 1,4-benzoquinone ($C_6H_4O_2$, D_2h) in Scheme 1 were used to calculate the NMR tensors at the same level of theory (B3LYP/6-311++G(d,p)) and referenced to benzene for ^{13}C (49.8 ppm, D_6h) and TMS for ^{1}H (31.981, T_d) as a standard according to [1]:

| Compound | -Reference (benzene) = Chemical shift (calculated) [1]

Given the experimental ^{13}C chemical shift of benzene in SO_2 relative to TMS (129.2 ppm)[5], correlation of the calculated ^{13}C-NMR chemical shifts with the experimental values provided very good agreement[6] according to:

Benzene Experimental – Chemical shift (calculated) [2]

The correlation of the calculated ^{1}H-NMR chemical shifts relative to TMS (0 ppm) according to [2] provides qualitative agreement with respect to the experimental chemical shifts (See Table S2).

Table S1: X-ray crystallographic data for **1**SbF_6•$C_6H_4O_2$, **3**$(AsF_6)_2$•CH_3CN and **3**$(SbF_6)_2$

	1SbF_6•$C_6H_4O_2$	**3**$(AsF_6)_2$•CH_3CN	**3**$(SbF_6)_2$
Formula	$C_{12}H_8F_6NO_4S_2Sb$	$C_8H_3As_2F_{12}N_3O_2S_4$	$C_6F_{12}N_2O_2S_4Sb_2$
a (Å)	9.0959(5)	18.343(4)	6.7574(12)
b (Å)	12.9028(7)	8.0690(13)	7.6967(14)
c (Å)	14.2415(8)	15.085(3)	17.669(3)
α (deg)	90.00	90.00	87.882(2)
β (deg)	93.500(1)	120.246(4)	88.198(2)
γ (deg)	90.00	90.00	70.539(2)
V (Å^3)	1680.02(16)	1928.9(6)	865.7(3)
Z	4	4	2
Space group	$P2_1/c$	C2/c	P-1
Cryst syst	monoclinic	monoclinic	triclinic
Color and habit	Black, Irregular	Colorless, Parallelepiped	Colorless, Parallelepiped
Fw	530.06	679.21	731.82
T (K)	173(1)	173(1)	173
λ (Å)	0.71073	0.71073	0.71073
ρ_{calcd} (Mg/m^3)	2.096	2.339	2.807
μ (mm^{-1})	1.973	4.024	3.733
reflns collected	8267	6425	6005
independent reflns	2856	2155	3757
R1, wR2	0.0221, 0.0539	0.0229, 0.0517	0.0270, 0.0690
Largest diff. peak and hole (e•Å^{-3})	0.702 and -0.268	0.499 and -0.264	1.096 and -1.073
CCDC	732426	732425	732427

1.3 Computational Details. Geometry optimizations and vibrational frequencies of all molecules were carried out using the B3LYP method[7] and the 6-311++G(d,p) basis set[8]. All structures were found to be minima as indicated by the absence of imaginary frequencies. NMR tensors were calculated using the GIAO method, while the single point free energies in solution were calculated using a polarization continuum model (PCM) with the integral equation formalism (IEF)[9], employing the PBE0 DFT hybrid functional[10] and using the gas-phase optimized structures (confirmed as minima by the absence of imaginary frequencies) as inputs. The following parameters were used to describe the solvent SO_2: dielectric constant (Eps) = 14.0, solvent radius (Rsolv) = 2.021 Å , molar volume (V(SO2)) = 46.75 Å^3 = 0.0468 nm^3 (used later in this paper), numeral density (q) = 0.01288 Å $^{-3}$, density =1.37027 g cm^{-3} as implement in *Gaussian 03W*.[4] Hyperfine coupling constants were calculated using the optimized structures and the B1LYP method[11,7b] and the EPR-II basis set[12] for all H, C, N, O atoms, while the 6-

31G(2d,p) basis set was used for S atoms as implemented in *Gaussian 98W*.[13] Vibrational frequencies were animated and assigned using *ChemCraft* Version 1.5.[14]

1.4. Syntheses. Caution! *Precautions should be taken to avoid explosion hazard when heating liquid SO_2 in a closed vessel (well ventilated fumehood, leather gloves, face shield, blast shield, carefully built pyrex vessel) and the use of pressure release valves are recommended. Arsenic pentafluoride (AsF_5) is extremely toxic and corrosive and should be handled in a well ventilated fumehood with a good metal vaccum line.*

1.4.1 General procedure for preparation of $1MF_6$ (M = As, Sb) according to Equation 1 in Scheme 1.[15]

In a typical reaction, $SNSMF_6$ (~ 5 mmol; ~ 1.57 g for M = Sb and ~ 1.34 g for M = As) and a slight excess (~ 5 %) of 1,4-benzoquinone (~ 5.5 mmol, ~ 0.595 g) were loaded into separate bulbs of a vessel of Type B (Figure S1b). A stir bar was added to the bulb containing 1,4-benzoquinone. SO_2 (~20-30 ml) was condensed onto reactants in bulb A and B. Upon warming to ambient temperature two yellow solutions were obtained in both bulb A and B. Small aliquots (~1-2 ml) of $SNSMF_6$ solution were gradually added to the stirring solution of 1,4-benzoquinone over 30 min. at ambient temperature. The solution gradually darkened from yellow-brown to a forest green solution with stirring for 2-4 hours. After stirring for an additional 8 hrs a deep royal blue solution is obtained. The volatiles were removed under dynamic vacuum giving a dark blue solid which was collected in the drybox, with isolated yields of 95-98 % (~ 2.06 g of **1**SbF_6 and ~ 1.85 g of **1**AsF_6 based on $SNSMF_6$ and Equation 1 in Scheme 1. The IR was checked as a Nujol mull on KBr plates (See Figure S2a (**1**AsF_6) and S3a (**1**SbF_6)) and are compared to the calculated IR frequencies in Table S9.

Comments:

1) The presence of the slight excess of 1,4-benzquinone used above in Section 1.4.1 can be detected by IR (c.f. ν C=O is 1685-1650; See Figure S2a and S3a)[16] and can be detrimental to further reactions if not removed (e.g. Section 1.4.4). However, the preparation of **3**$(MF_6)_2$ according to Equation 2-4 in Scheme 1 (Section 1.4.11) is not affected by the presence of 1,4-benzoquinone.

2) The use of excess 1,4-benzoquinone in Section 1.4.1 is recommended for large scale (> 5 mmol) preparation of **1**SbF_6, however the use of very pure $SNSMF_6$ and small scales (~ 1 mmol) in dilute solution leads to analytically pure **1**MF_6.[15]

Equation 1 according to Scheme 1:

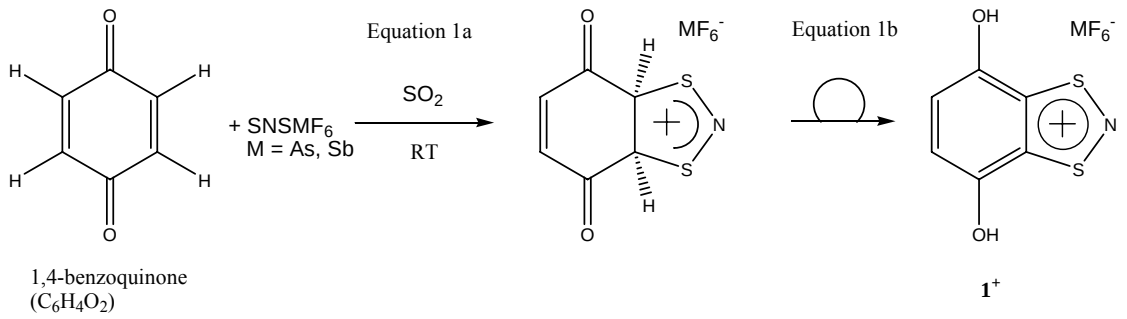

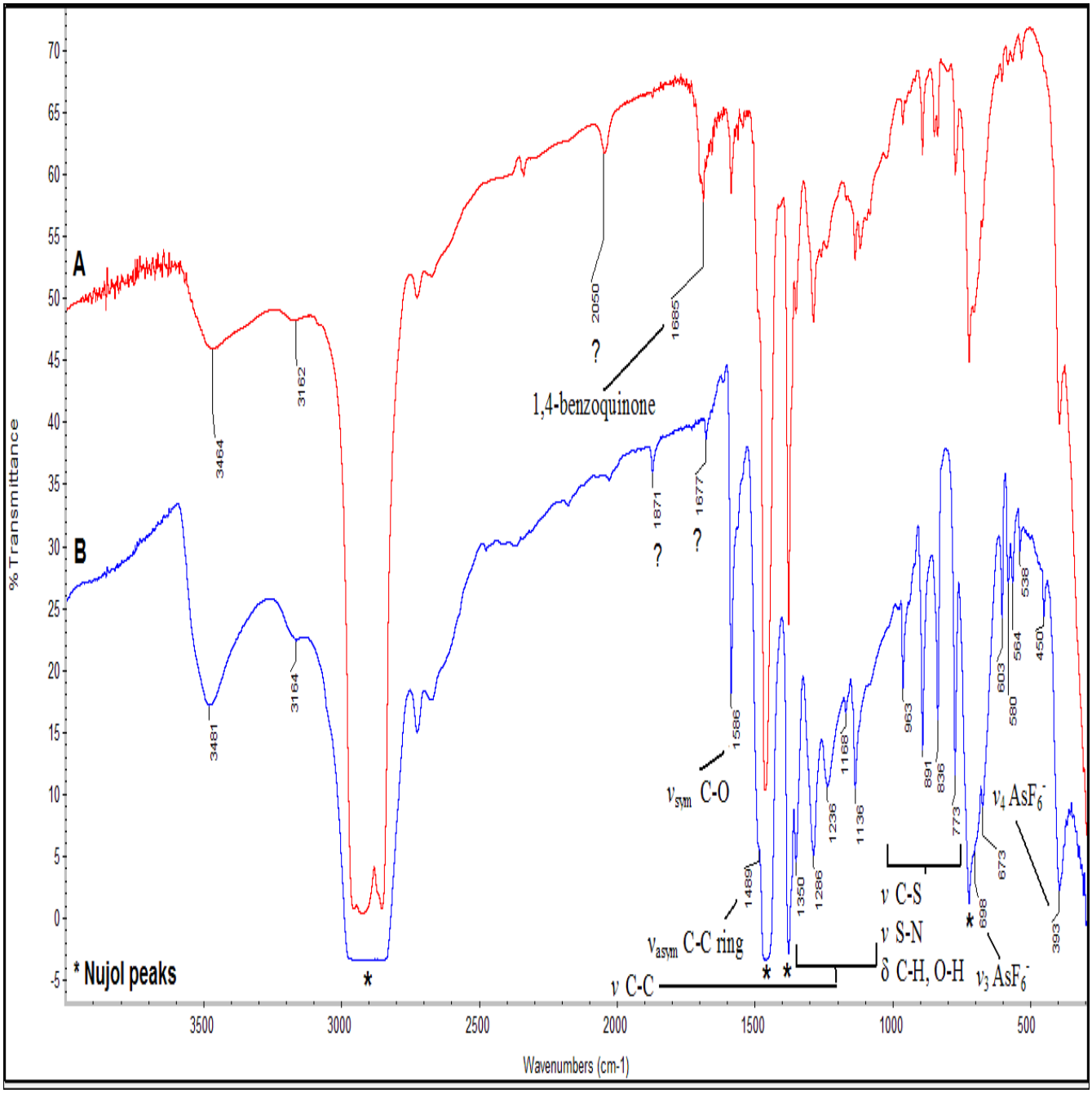

Figure S2: FT-IR of a) crude **1**AsF_6 and b) purified **1**AsF_6 as Nujol mull on KBr plates (32 scans, 2 cm^{-1} resolution). See Table S9 for comparison of experimental and calculated IR frequencies and tentative assignments (Note the tentative assignments: ν = stretch, δ =bending, asym. = asymmetric and sym = symmetric):

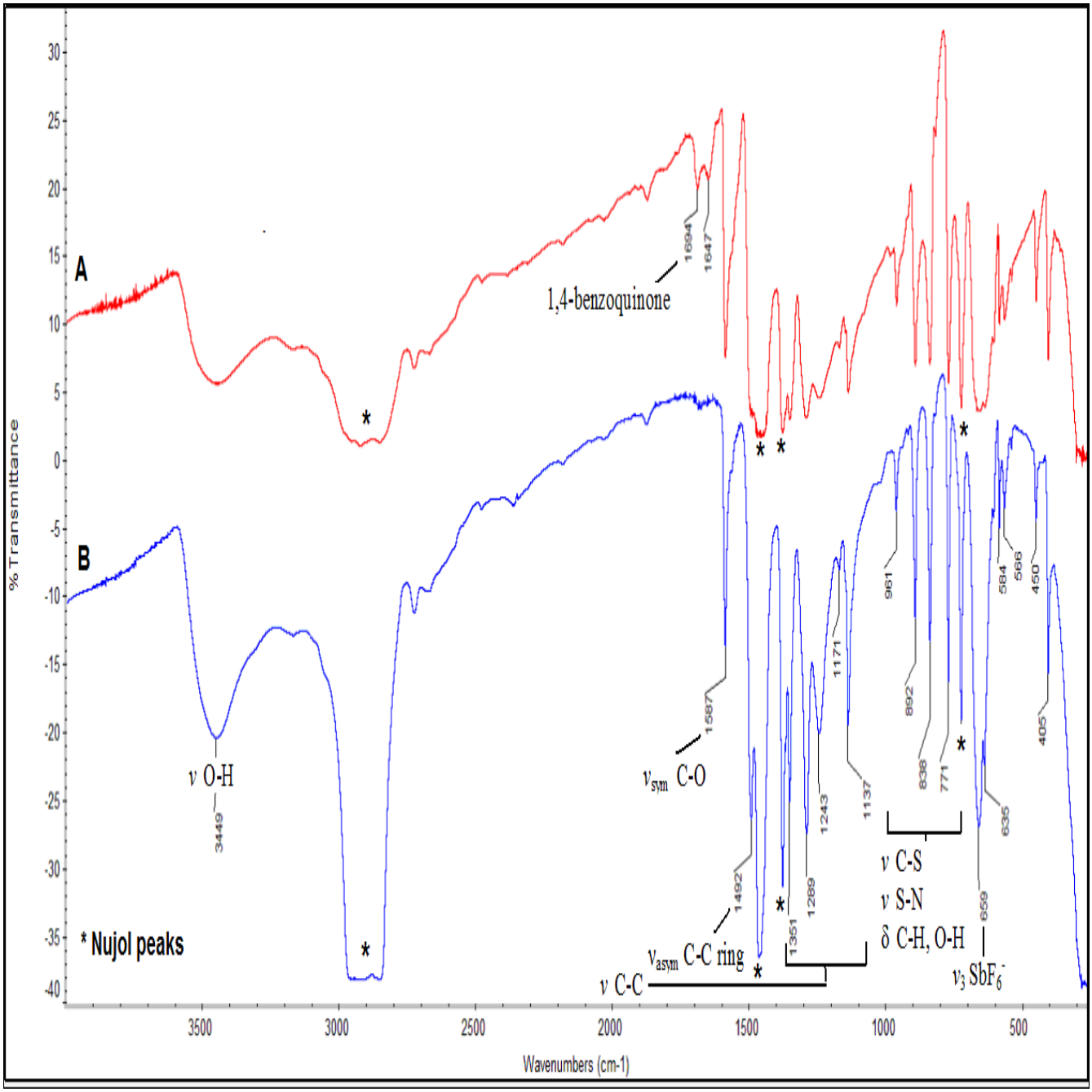

Figure S3: FT-IR of a) crude **1**SbF_6 and b) purified **1**SbF_6 as Nujol mull on KBr plates (32 scans, 2 cm^{-1} resolution). See Table S9 for comparison of experimental and calculated IR frequencies and tentative assignments (Note the tentative assignments: ν = stretch, δ =bending, asym. = asymmetric and sym = symmetric):

1.4.2 General procedure for purification of 1MF_6 (M = As, Sb) prepared according to Equation 1 in Scheme 1

1MF_6 (~ 5 mmol) was added to bulb A of a vessel of type B (Figure S1b). CH_3CN (~ 1 ml per mmol of **1**(MF_6)) and CH_2Cl_2 (~ 5 ml per ml of CH_3CN) were condensed consecutively into bulb A and bulb B, respectively. On warming to ambient temperature a dark blue solution is obtained in bulb A. Typically all of **1**MF_6 should be dissolved,

however the more soluble fraction is filtered into bulb B containing CH_2Cl_2. A blue precipitate under a blue-black solution was obtained. After standing for 12 hrs the more soluble fraction was filtered to bulb A. The volatiles were removed from the more soluble fraction under dynamic vacuum. CH_2Cl_2 (~ 5 ml) is condensed on to the blue precipitate in bulb B. The blue precipitated was washed with the CH_2Cl_2 and the more soluble fraction filtered to bulb A. The volatiles were condensed back to bulb B and the more soluble fraction filtered to bulb A. This was repeated twice more and the volatiles removed under dynamic vacuum. The blue precipitate in bulb B (**1**MF_6, ~ 3.5-4 mmol; ~1.47g of M = Sb and ~ 1.32 g of M = As) is typically recovered in 70-80% yield. The IR was checked as a Nujol mull on KBr plates (See Figure S2b (**1**AsF_6) and S3b (**1**SbF_6)). See the comparison of experimental and calculated frequencies for **1**SbF_6, **1**AsF_6 and **1**SbF_6•$C_6H_4O_2$ (Section 1.4.7) in Table S9.

Comments:

1) The IR indicate the absence of 1,4-benzoquinone (c.f. ν C=O is 1685-1650; See Figure S2b and S3b) which remains in the more soluble fraction (e.g. ν C=O is 1685-1650 Figure S2a and Figure S3a).[16] Furthermore, the removal of 1,4-benzoquinone leads to better resolution of the frequencies assigned to **1**MF_6 between 1500-1000 cm^{-1} (See Figures S2b and S3b).

2) The more soluble fractions are collected and can be further purified as described above. However, we note the presence of substantial quantities of 1,4-benzoquinone leads to the 1:1 lattice inclusion complex **1**SbF_6•$C_6H_4O_2$ (c.f. Section 1.4.3) which is substantially more soluble in CH_2Cl_2 and results in reduced yields (~ 40-50%) of **1**MF_6 according to the procedure described above in Section 1.4.2.

1.4.3 *In situ* multinuclear NMR of the reaction of 1SbF_6 with excess $SNSSbF_6$ in SO_2 according to Equation 2-4 in Scheme 1

1SbF_6 (0.422 g, 1.00 mmol) and $SNSSbF_6$ (0.718 g, 2.29 mmol) were loaded in to a 10 mm NMR tube (Type D). SO_2 (5.174 g) was condensed on to the solids and the NMR tube flame sealed. A dark blue solution was obtained on warming to ambient temperature. The multinuclear NMR (^1H, ^{13}C, ^{14}N) was followed over 36 hours and check again after 9 and 22 days. After an additional 2 months standing at 25 ^oC several clear colorless crystals were isolated from the NMR tube and identified as **3**$(SbF_6)_2$ by single crystal X-ray diffraction. The X-ray structure of **3**$(SbF_6)_2$ is given in Figure S7 and the two SbF_6^- anions are illustrated in Figure S8 with bond lengths (Å) and angles (^{o}). The experimental and calculated bond lengths (Å) and angles (^{o}) are compared in Table S3 (See Table S1 in Section 1.2 for details on X-ray crystallographic data). The actual multinuclear NMR spectra are given in Figure S4-S6 with assignments (See interpretation below).

^{1}H-NMR: The initial ^{1}H-NMR (Figure S4) showed two singlet resonances assigned to δ(C-H) and δ(O-H) of **1**$^+$ and a 1:1:1 triplet centered at δ 5.8 of NH_4^+ and an unassigned 1:1:1 triplet centered at δ 6.6 and two unassigned singlet resonances at δ 4.3 and δ 3.5. After 36 hours, the triplet centered at δ 6.6 could not be observed, but a new resonance at δ 7.3, tentatively assigned to **5**$^•$ could be observed (See Figure S4 and the corresponding interpretation of ^{13}C-NMR given below). After 9-22 days no new resonances appear in the ^{1}H-NMR (Figure S4).

However, the integration ratio of $\mathbf{1}^+$ (δ 7.7-7.0) to NH_4^+ (δ 6.2-5.6) is 5.5:1 in the initial ^{1}H-NMR which corresponds to ~ 15 % formation of $\mathbf{3}^{2+}$ according to Equation 2-4 in Scheme 1. After 36 hrs the ratio of $\mathbf{1}^+$ to NH_4^+ is 4:1 (~ 20 % formation of $\mathbf{3}^{2+}$, Equation 2-4 in Scheme 1), while after 9-22 days the ratio is relatively unchanged at ~2:1 corresponding to ~ 35 % formation of $\mathbf{3}^{2+}$ (Equation 2-4 in Scheme 1) after three weeks at ambient temperature.

^{13}C-NMR: The initial ^{13}C-NMR (Figure S5) is consistent with the previously reported $\mathbf{1}^+$ (c.f. δ 154.5, 146.3 and 120.2).[15] After 36 hours the coupled ^{13}C-NMR was obtained and resonances assigned to $\mathbf{1}^+$ were observed,[15] while three new resonances (δ 177.3 (C-S), 162.2 (C=O) and 140.2 (C-H, $J_{C\text{-}H}$ = 184 Hz)) are tentatively assigned to $\mathbf{5}^{\bullet}$ (Chart 1) based on the calculated ^{13}C-NMR given in Table S2. The ^{13}C-NMR remains unchanged after 9-22 days.
Comment: $\mathbf{7}^{2+}$ and $\mathbf{8}^{2+}$ (Scheme 1) could not be observed in solution at ambient temperature. This suggests the reaction is relatively sluggish at ambient temperature according to Equation 2-4 in Scheme 1.

^{14}N-NMR: The initial ^{14}N-NMR (Figure S6 shows three assignable resonances to δ -12.1 (c.f. δ -7.4 for $\mathbf{1}^+$) and comparable to related 1,3,2-dithiazolyliums, δ -95.9 SNS^+ (c.f. δ -95)[17], and a 1:1:1 triplet centered at δ -364.7 NH_4^+. The ^{14}N-NMR after 9-22 days is relatively unchanged. The integration ratio of $\mathbf{1}^+$ relative to NH_4^+ were ~ 3:1, consistent with ~ 33 % formation of $\mathbf{3}^{2+}$ according to Equation 2-4 in Scheme 1. This is consistent with the integration of $\mathbf{1}^+$ relative to NH_4^+ in the ^{1}H-NMR (c.f. ~ 35 %). We note the integration of δ -12.1 assigned to $\mathbf{1}^+$ increases from 15.7% to 23.1 %, which may be attributed to the presence of 1,4-benzoquinone in $\mathbf{1}SbF_6$ (See Section 1.4.1 and Comment 1).

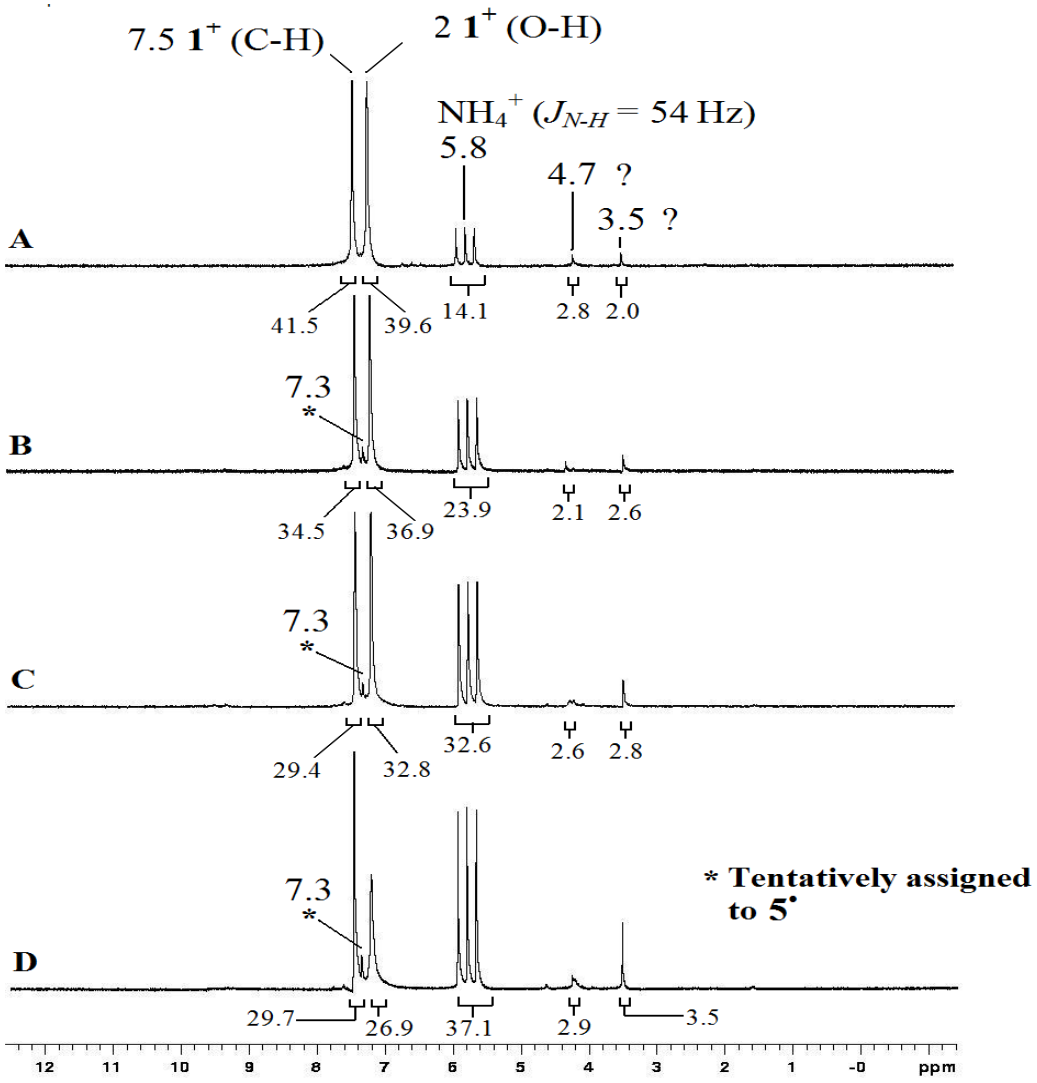

Figure S4: ^{1}H-NMR of the *in situ* NMR reaction of **1**SbF_6 with excess $SNSbF_6$ in liquid SO_2 at 25 ^{o}C. Assignments are made in **A** and integration of each resonance are given below each spectra; **A**: Initial, **B**: After 36 hours, **C**: After 9 days and **D**: After 3 weeks (See Section 1.4.3 for Experimental and Discussion).

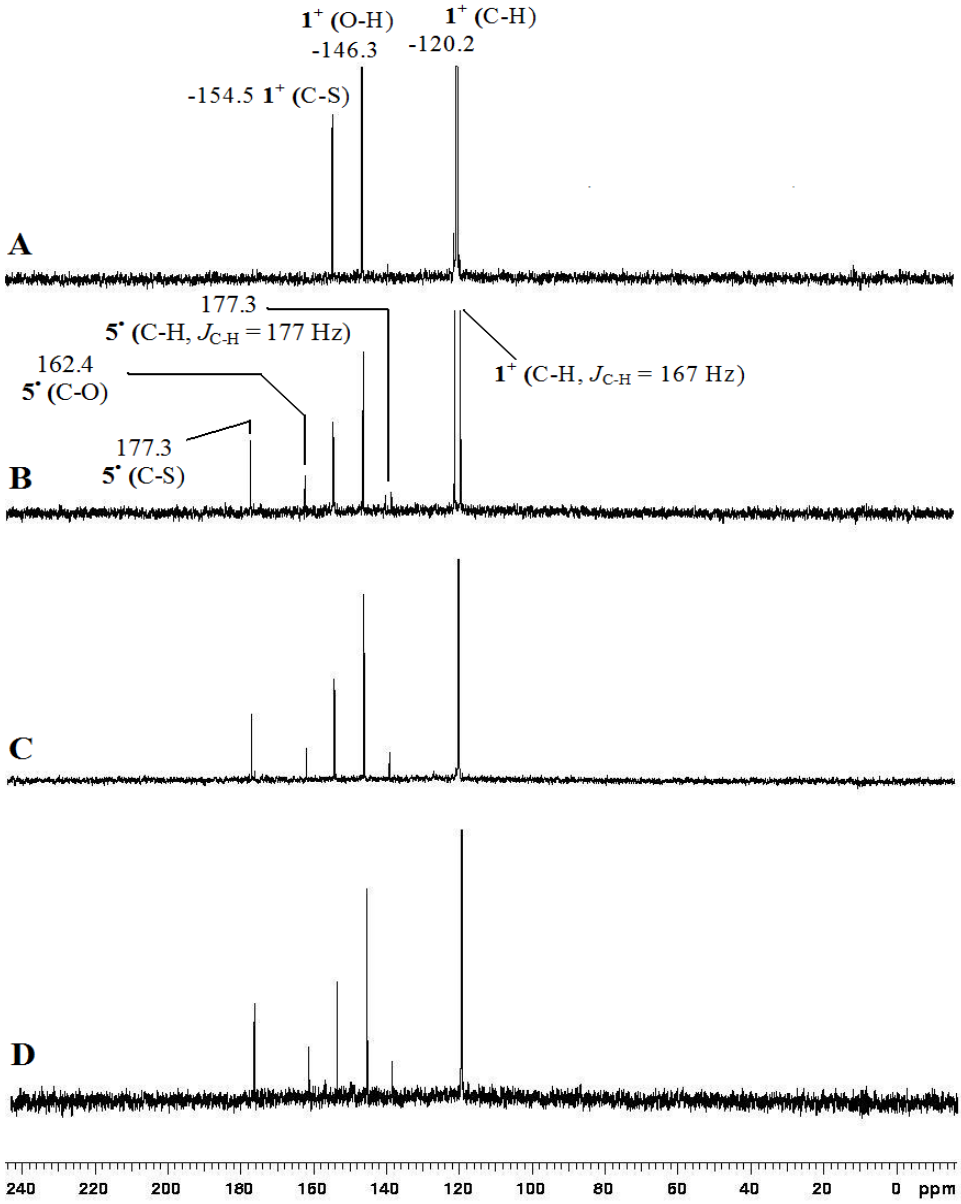

Figure S5: ^{13}C-NMR of the *in situ* NMR reaction of **1**SbF_6 with excess $SNSSbF_6$ in liquid SO_2 at 25 ^{o}C. Assignments are made in **A** and **B** where **A**: Initial, **B** (coupled ^{1}H-^{13}C NMR): After 36 hours, **C**: After 9 days and **D**: After 3 weeks (See Section 1.4.3 for Experimental and Discussion).

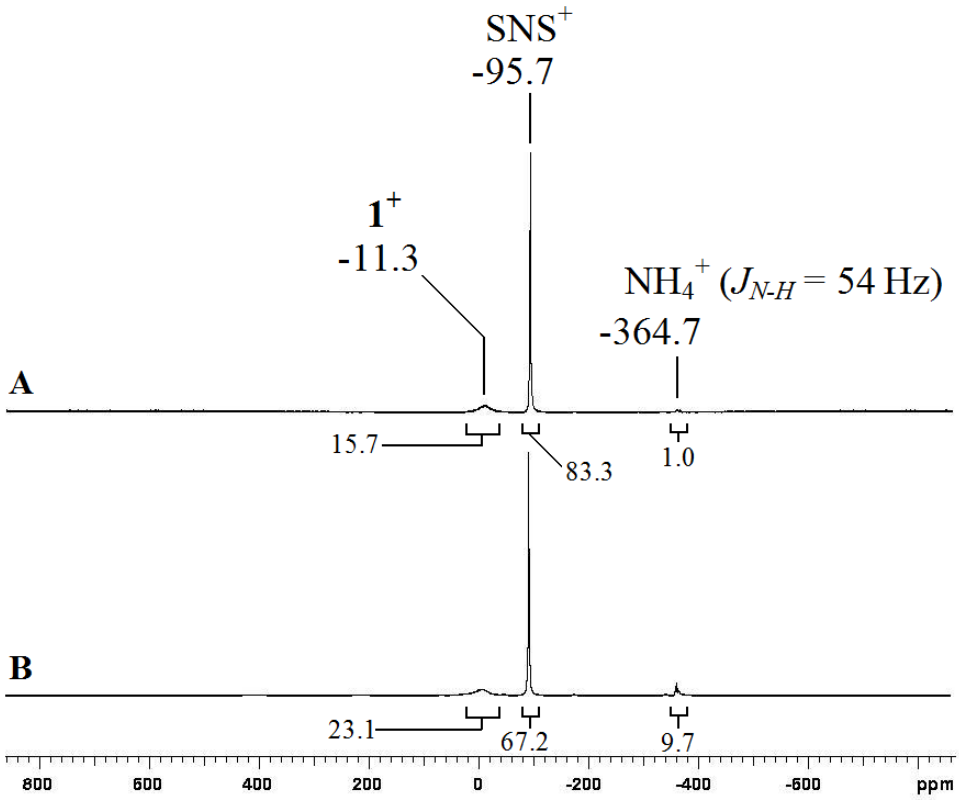

Figure S6: ^{14}N-NMR of the *in situ* NMR reaction of **1**SbF_6 with excess $SNSSbF_6$ in liquid SO_2 at 25 ^{o}C. Assignments are made in **A** where **A**: Initial, **B** After 22 days (See Section 1.4.3 for Experimental and Discussion).

Table S2: Comparison of calculated (B3LYP/6-311++G(d,p)) and experimental ^{13}C and ^{14}N-NMR tensors of $\mathbf{1}^+$, $\mathbf{5}^+$, $\mathbf{5}^{\bullet}$ $\mathbf{3}^{2+}$, $\mathbf{7}^{2+}$, $\mathbf{8}^{2+}$ and **1**,4-benzoquinone ($C_6H_4O_2$) (Atom

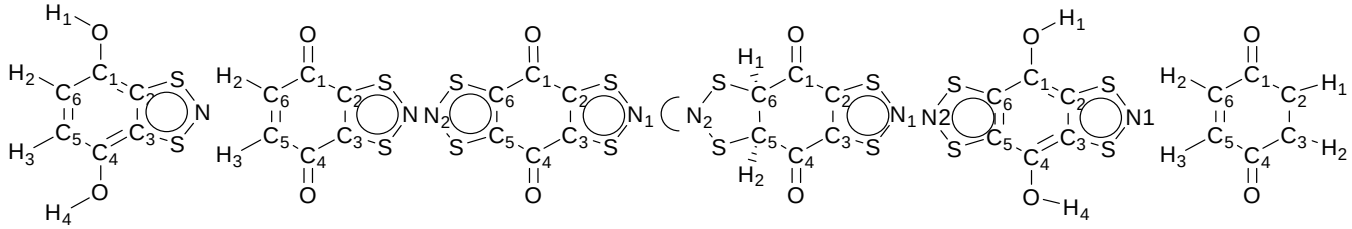

$\mathbf{1}^+$ $\mathbf{5}^+$ $\mathbf{3}^{2+}$ $\mathbf{7}^{2+}$ $\mathbf{8}^{2+}$ **1,4-benzoquinone $C_6H_4O_2$**

labelling given below):

Compound	$\mathbf{1}^+$		$\mathbf{5}^+$		$\mathbf{5}^{\bullet}$		$\mathbf{3}^{2+}$		$\mathbf{7}^{2+}$		$\mathbf{8}^{2+}$		**1,4-benzoquinone ($C_6H_4O_2$)**	
Molecular Symmetry	C_{2v}		C_{2v}		C_{2v}		C_2		C_1		C_1		D_2h	
Atom	Calc.	Exp.	Calc.	Exp.	Calc.	Exp.	Calc.[b]	Exp.[a]	Calc.	Exp.	Calc.	Exp.	Calc.	Exp.
C1	148.5	146.5	175.1	175.1	178.2	177.3	168.1	156.0	176.7	NA	143.9	NA	166.9	188.7
C2	156.9	154.8	176.6	177.2	157.5	162.2	181.0	178.6	177.5	NA	154.6	NA	136.6	136.9
C3	156.9	154.8	176.6	177.2	157.5	162.2	181.0	178.6	177.9	NA	160.8	NA	136.6	136.9
C4	148.5	146.5	175.1	175.1	178.2	177.3	168.1	156.0	172.6	NA	143.9	NA	166.9	188.7
C5	117.9	119.5	117.4	140.0	137.6	139.3	181.0	178.6	81.9	NA	160.8	NA	136.6	136.9
C6	117.9	119.5	117.4	140.0	137.6	139.3	181.0	178.6	78.2	NA	154.6	NA	136.6	136.9
H1	5.62	7.52									7.28		6.75	6.81
H2	7.44	7.96	7.66	8.25	6.73	7.32			6.25	NA			6.75	6.81
H3	7.44	7.96	7.66	8.25	6.73	7.32			6.44	NA			6.75	6.81
H4	5.62	7.52									7.28		6.75	6.81
N1 [c]	0 [c]	-7.4 (ref 15)	7.6	1.8	-221.2	NA	46	NA	46.8	NA	66.9	NA		
N2 [c]							46	NA	139.6	NA	66.9	NA		

[a] NMR was obtained in CD_3CN. [b] Calculated relative to benzene in SO_2. [c] The ^{14}N-NMR are calculated relative to $\mathbf{1}^+$ (Used as a reference and has a calculated chemical shift of -223.2 ppm) by the following Equation: | Compound – $\mathbf{1}^+$ (c.f. -223.2 ppm) | = Calculated ^{14}N –NMR.

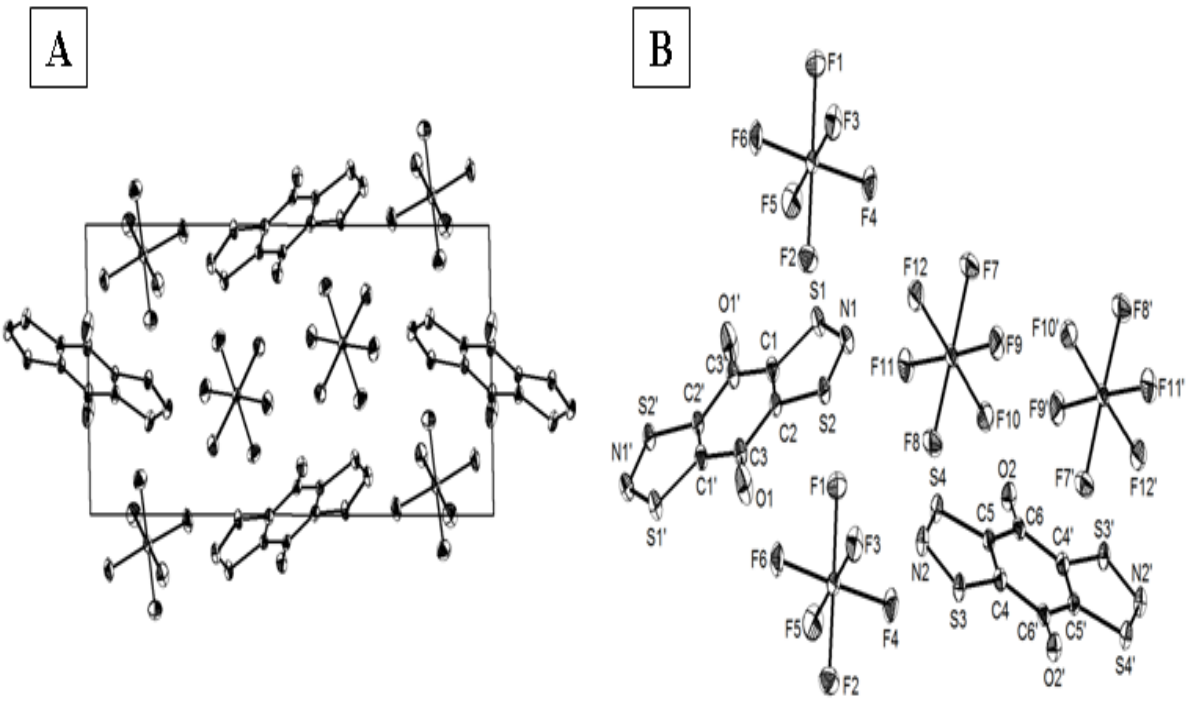

Figure S7: The X-ray crystal structure of **3**$(SbF_6)_2$ where a) a view of the unit cell along the b-axis and b) the atom labelling within the asymmetric unit. Thermal ellipsoids are given at 50 % probability. A comparison of experimental and calculated bond distances and angles are given in Table S3.

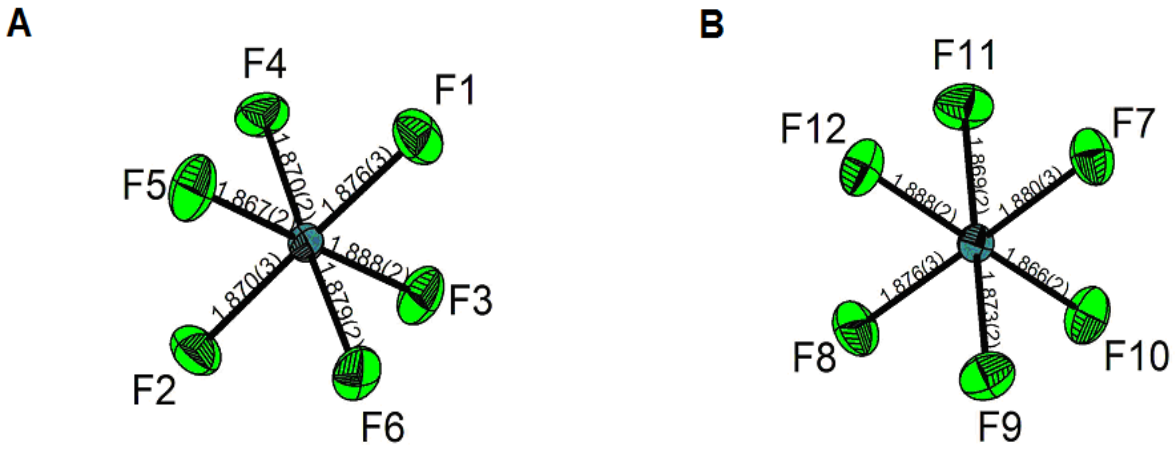

A: F1-Sb1-F2 = 179.01 (10), F1-Sb1-F3 = 89.38(10), F1-Sb1-F4 = 91.43(10), F1-Sb1-F5 = 90.34(11), F1-Sb1-F6 = 88.32(10), F2-Sb1-F3 = 90.33(10), F2-Sb1-F4 = 89.52(11), F2-Sb1-F5 = 89.96(11), F2-Sb1-F6 = 90.72(10), F3-Sb1-F4 = 88.87(10), F3-Sb1-F5 = 179.25(10), F3-Sb1-F6 = 88.02(10), F4-Sb1-F5 = 90.44(11), F4-Sb1-F6 = 176.89(9), F5-Sb1-F6 = 92.67(11).

B: F7-Sb2-F8 = 177.67(10), F7-Sb2-F9 = 88.51(10), F7-Sb2-F10 = 92.04(10), F7-Sb2-F11 = 90.29(11), F7-Sb2-F12 = 88.41(10), F8-Sb2-F9 = 90.64(10), F8-Sb2-F10 = 90.16(10), F8-Sb2-F11 = 90.50(10), F8-Sb2-F12 = 89.40(10), F9-Sb2-F10 = 92.80(9), F9-Sb2-F11 = 177.97(10), F9-Sb2-F12 = 88.69(10), F10-Sb2-F11 = 88.87(10), F10-Sb2-F12 = 178.45(10), F11-Sb2-F12 = 89.65(10).

Figure S8: The two slightly distorted SbF_6^- anions **A** and **B** in **3**$(SbF_6)_2$ with bond distances (Å) and bond angles (^{o}).

Table S3: Comparison of calculated (B3LYP/6-311++G(d,p)) and experimental bond lengths (Å) and angles (°) of $\mathbf{3}^{2+}$ and $\mathbf{3}^{+\bullet}$ in $\mathbf{3}(AsF_6)_2 \bullet CH_3CN$ and $\mathbf{3}(SbF_6)_2$ (Atom labelling is given to right):

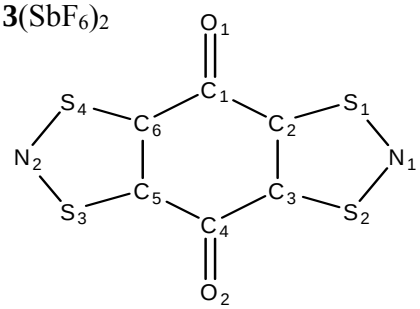

Bond	$\mathbf{3}(SbF_6)_2$		$\mathbf{3}(AsF_6)_2 \bullet CH_3CN$	Calc.[a] $\mathbf{3}^{2+}$	Calc.[a] $\mathbf{3}^{+\bullet}$
Bond Length (Å)					
O1-C1	1.201(6)	1.199(5)	1.203(2)	1.199	1.233
O2-C4	1.201(6)	1.199(5)	1.203(2)	1.199	1.233
C1-C2	1.487(5)	1.500(5)	1.493(2)	1.502	1.459
C2-C3	1.372(5)	1.370(5)	1.371(2)	1.372	1.400
C3-C4	1.496(5)	1.497(4)	1.491(2)	1.502	1.459
C4-C5	1.487(5)	1.500(5)	1.493(2)	1.502	1.459
C5-C6	1.372(5)	1.370(5)	1.371(2)	1.372	1.400
C6-C1	1.496(5)	1.497(4)	1.491(2)	1.502	1.459
C2-S1	1.701(3)	1.699(3)	1.694(2)	1.737 [b]	1.732 [b]
S1-N1	1.599(4)	1.603(4)	1.599(2)	1.611	1.616
S2-N1	1.604(4)	1.605(3)	1.599(2)	1.611	1.616
C3-S2	1.698(3)	1.699(3)	1.701(2)	1.737 [b]	1.732 [b]
C5-S3	1.701(3)	1.699(3)	1.694(2)	1.737 [b]	1.732 [b]
S3-N2	1.599(4)	1.603(4)	1.599(2)	1.611	1.616
S4-N2	1.604(4)	1.605(3)	1.599(2)	1.611	1.616
C6-S4	1.698(3)	1.699(3)	1.701(2)	1.737 [b]	1.732 [b]
Bond Angles (°)					
O1-C1-C2	123.8(3)	123.6(3)	122.25(3)	123.21	123.21
O1-C1-C6	122.7(3)	123.5(3)	124.25(2)	123.21	123.21
O2-C4-C3	122.7(3)	123.5(3)	124.25(2)	123.21	123.21
O2-C4-C5	123.8(3)	123.6(3)	122.25(3)	123.21	123.21
C1-C2-C3	123.1(3)	123.6(3)	123.78(3)	123.20	123.20
C2-C3-C4	123.3(3)	122.6(2)	122.63(2)	123.20	123.20
C3-C4-C5	113.5(3)	112.9(3)	113.46(3)	113.58	113.58
C4-C5-C6	123.1(3)	123.6(3)	123.78(3)	123.20	123.20
C5-C6-C1	123.3(3)	122.6(2)	122.64(2)	123.20	123.20
C6-C1-C2	113.5(3)	112.9(3)	133.46(3)	113.58	113.58
C1-C2-S1	123.5(2)	122.6(2)	122.61(3)	123.11	123.11
C2-S1-N1	98.3(2)	98.5(2)	98.35(3)	97.09	97.09
C2-C3-S2	113.6(3)	113.8(3)	113.60(2)	113.98	113.68
C3-S2-N1	98.1(2)	98.1(2)	98.35(3)	97.09	97.09
C3-C2-S1	113.3(2)	113.2(2)	113.60(2)	113.68	113.68
S1-N1-S2	116.6(2)	116.3(2)	116.55(2)	118.45	118.45
C4-C3-S2	123.0(2)	123.2(2)	123.99(3)	123.11	123.11
C4-C5-S3	123.0(2)	123.2(2)	123.99(3)	123.11	123.11
C5-S3-N2	98.3(2)	98.5(2)	98.35(3)	97.09	97.09
C5-C6-S4	113.6(3)	113.8(3)	113.60(2)	113.98	113.68
C6-S4-N2	98.1(2)	98.1(2)	98.35(3)	97.09	97.09
C6-C5-S3	113.3(2)	113.2(2)	113.60(2)	113.68	113.68
S3-N2-S4	116.6(2)	116.3(2)	116.55(2)	118.45	118.45
C1-C6-S4	123.5(2)	122.6(2)	122.61(3)	123.11	123.11

[a] Gas phase structures calculated using the B3LYP method and 6-311++G(d,p) basis set.
[b] DFT methods tend to over estimate the C-S bond length in related thiazyl compounds.[18]

1.4.4 Reaction of 1SbF_6 with excess $SNSSbF_6$ in SO_2 according to Equation 2-4 in Scheme 1

1(SbF_6) (2.122 g, 5.03 mmol) and $SNSSbF_6$ (3.816 g, 12.16 mmol) were added into bulb A of a vessel of Type A (Figure S1a) with a Teflon coated stir bar. SO_2 (57.732 g, ~ 40 ml) was condensed into bulb A. A dark blue solution was obtained on warming to ambient temperature and was stirred continuously. After 1 week a blue solution over a small quantity of black insoluble was observed. A trace of Br_2 (0.089 g, 1.11 mmol) was condensed into the mixture and warm to ambient temperature. The condenser was cooled with running water and the reaction mixture gently refluxed with an external electric heating mantle at ~ 50-60 ^oC (Note the valve to bulb B was closed during the reflux). After refluxing for 1 week, a blue-black solution over a grey insoluble is obtained. The solution was allowed to cool to ambient temperature and the more soluble fraction filtered to bulb B. The volatiles (~ 10 ml) were condensed back to bulb A and the more soluble fraction filtered into bulb B. This was repeated until the more soluble fraction was colorless. The volatiles were removed under dynamic vacuum and the condenser rinsed with acetone and dried with a stream of air before collecting the solids in the drybox. The grey insoluble in bulb A (3.227 g, 81 % yield of **3**$(SbF_6)_2$ based on **1**SbF_6 and Equation 2-4 in Scheme 1) and the more soluble fraction from bulb B (2.637 g) were collected. The IR of the grey insoluble as a Nujol mull was obtained on KBr plates and were consistent with **3**$(SbF_6)_2$ (Figure S9a) based on comparison to the calculated IR frequencies and intensities in Table S4. The elemental analysis of the grey insoluble:
Found C 7.18%, N 3.94%, S 16.85%, F 30.73%, Sb 34.9%;
Calculated based on 1/8 S_8 in Equation 2-4 in Scheme 1: C 7.55%, N 4.03%, S 16.80%, F 32.85%, Sb 35.09% (See Equation 6b below were $SNSAsF_6$ oxidizes sodium dithionite ($Na_2S_2O_4$)).
Calculated based on **3**$(SbF_6)_2$: C 9.85%, N 3.83%, S 17.53%, F 31.15%, Sb 33.27%;

Comments:

1) We note the satisfactory agreement of the elemental analysis of the grey insoluble and the reasonable agreement with Equation 2-4 in Scheme 1 and only 1/8 S_8. While this supports the proposed reaction scheme given in Scheme 1 (above) and is supported by the gas phase and solution phase (SO_2) calculations (Table S5). We recognized the possibility that the oxidative dehydrogenation of SNS^+ according to Equation 2-4 in Scheme 1 is more complicated. We note the reaction of SNS^+ with a range of reducing agents has lead to different identified products as outlined in Equation 6a-c[19] which may account for the deficit of S_8 (e.g. Equation 6b) determined by elemental analysis according to Equation 2-4 in Scheme 1 (above).

Equation 6:

[a] $2\ SNSAsF_6 + 2\ KI \rightarrow S_{1.5}NI_{1.5} + 2\ KAsF_6 + ¼\ I_2 + {}^5/_8\ S_8 + ½\ N_2$

[b] $2\ SNSAsF_6 + ½\ Na_2S_2O_4 \rightarrow S_3N_2AsF_6 + NaAsF_6 + SO_2 + {}^1/_8\ S_8$

[c] $SNSAsF_6 + CsN_3 \rightarrow (SN)_x + CsAsF_6 + N_2$

However, we note that there is no evidence of the formation of SN_x (Equation 6c) by qualitative EDX microanalysis by scanning electron microscopy (SEM) (Figure S11) which shows no indication of the presence of N, but the formation of S_8 (c.f. Equation 2-4 in Scheme 1) has been confirmed by Raman microcscopy (Figure S10) and EDX microanalysis by scanning electron microscopy (SEM) as shown in Figure S11.

Overall summary of Equation 2-4 in Scheme 1:

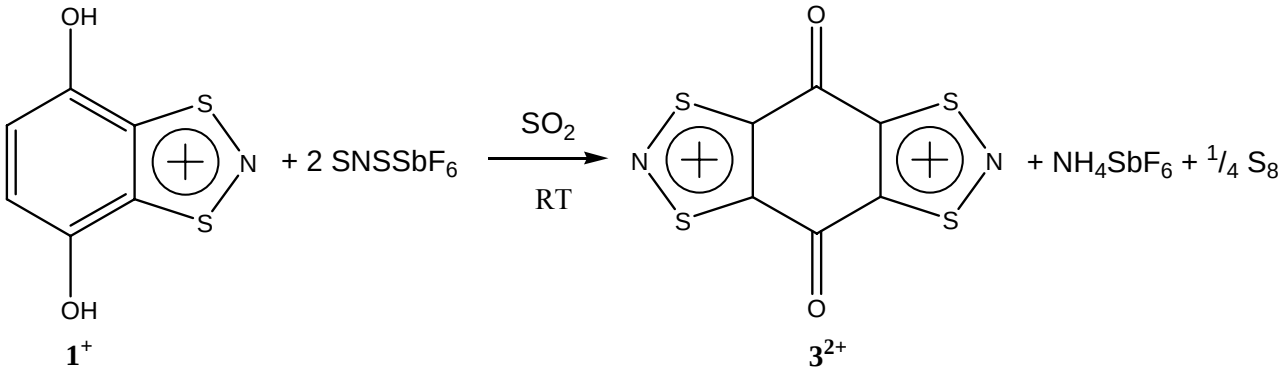

1^{+} **3**$^{2+}$

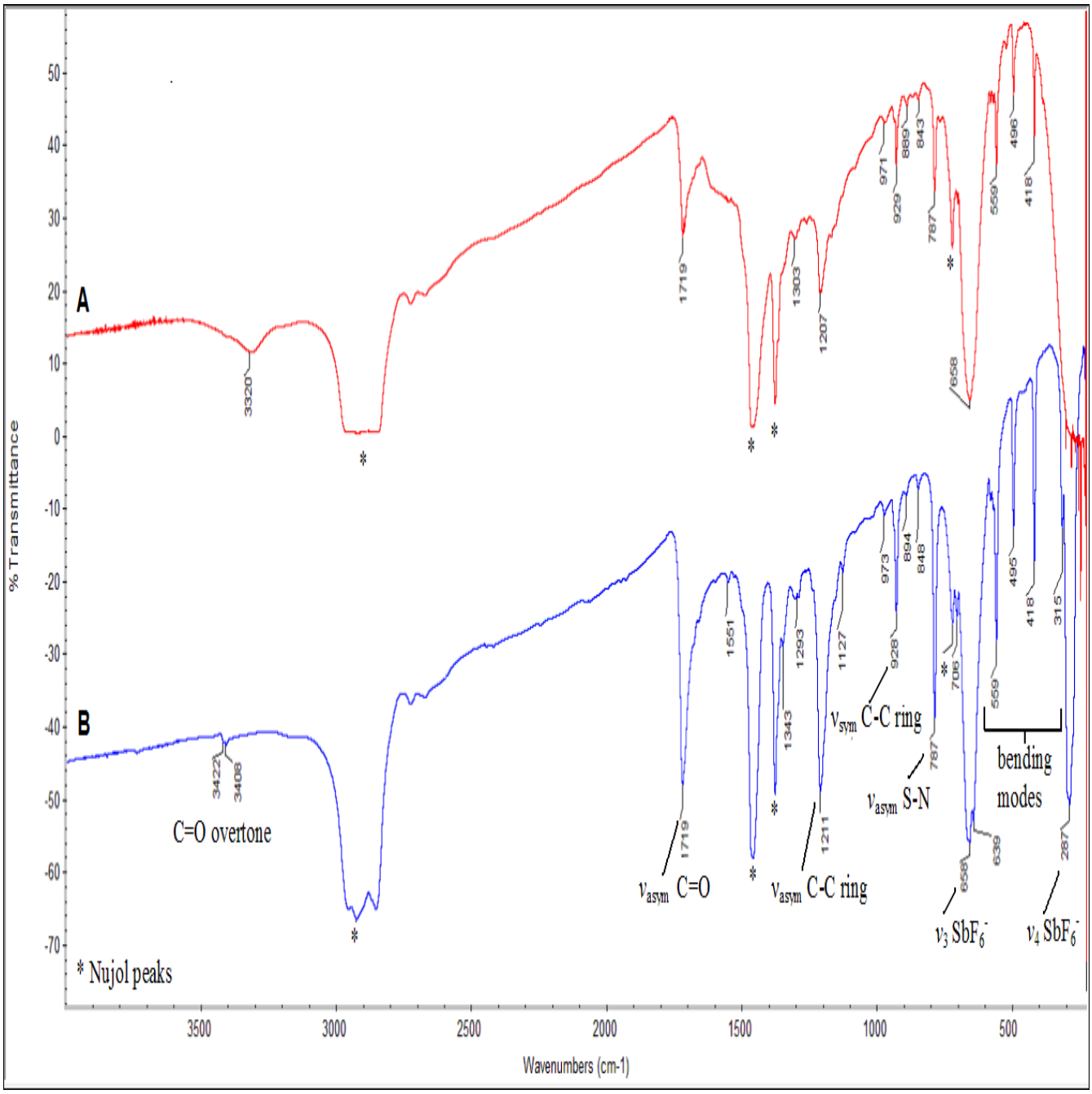

Figure S9: The FT-IR of a) crude **3**$(SbF_6)_2$ on KBr plates and b) purified **3**$(SbF_6)_2$ on CsI plates (32 scans, 2 cm^{-1} resolution). See Table S4 for comparison of experimental and calculated IR frequencies and tentative assignments (Note the tentative assignments: ν = stretch, δ =bending, asym. = asymmetric and sym = symmetric):

Table S4: Comparison of calculated (B3LYP/6-311++G(d,p)) and experimental IR frequencies for $\mathbf{3}^{2+}$ and $\mathbf{3}^{+\bullet}$.

3$(SbF_6)_2$			Tentative Assignments [a]	**3**SbF_6		Tentative Assignments [a]
IR/Raman (Calc.)	IR [b] **3**$(SbF_6)_2$ (Obs.)	IR [e] **3**$(AsF_6)_2$ (Obs.)		IR/Raman (Calc.)	IR [b,e] (Obs.)	
	3315s,br	3325s,br	NH_4^+			
1723 (63/0) [d]	1718s	1718s	ν_{asym} C=O		1720s	ν_{asym} C=O of $\mathbf{3}^{2+}$
1715 (0/100) [d]						
				1618 (0/27) [d]		
				1526 (88/0) [d]	1595m	ν_{sym} C-O of $\mathbf{3}^{+\bullet}$
1500 (0/60)				1438 (0/14)		
1476 (9/0)	1306w	1305w				
				1340 (44/0)	1313s	ν_{asym} C=C of $\mathbf{3}^{+\bullet}$
				1337 (0/100)		
1282 (0/8)	1265vw					
		1258w				
1180 (100/0)	1208s	1206s	Asym. νC-C + νC-S	1139 (2/0)	1208s	Asym. νC-C + νC-S of $\mathbf{3}^{2+}$
	1175w,sh	1173w,sh				
1172 (6/0)	1151w,sh		ν_{asym} C-C ring		1151m	ν_{asym} C-C ring of $\mathbf{3}^{2+}$
				1092 (49/0)		
	1078w,sh	1079w,br				
	1019w	1026w				
984 (0/28)	972w	970w	$\nu_{sym.}$ C-S	952 (1/0)	971w	$\nu_{sym.}$ C-S of $\mathbf{3}^{2+}$
953 (0/7)	930m	929m	Sym. νC-C + νC-S	940 (0/21)		
951 (1/0)						
929 (4/0)	891w	892w			929m	
					894m	
844 (0/6)	841w	847w				
				867 (0/17)		
				808 (100/0)		
				776 (6/0)		
776 (22/0)	787m	789m	ν_{asym} S-N	762 (0/6)	787m	ν_{asym} S-N of $\mathbf{3}^{2+}$
					772m	
				748 (0/1)		
743 (0/1)						
742 (0/17)						
722 (4/0)						
711 (0/3)				707 (3/0)		
677 (3/0)				689 (1/0)		
		696vs,br	ν_3 AsF_6^-			
		661m,sh	ν_{asym} C-S			
	660vs,br		ν_3 SbF_6^-		657vs	ν_3 SbF_6^-
				640 (0/1)		
587 (0/20)				585 (0/1)		
576 (8/0)	559m	561m	δ_{asym} S-N-S bending	573 (2/0)		
					559w	δ_{asym} S-N-S bending of

						$\mathbf{3}^{2+}$
				487 (0/1)		
484 (2/0)	494m	496m	Inp. Ring bending		496m	Inp. Ring bending of $\mathbf{3}^{2+}$
471 (0/6)						
445 (1/0)				447 (6/0)		
437 (0/1)				429 (0/1)		
425 (6/0)	417m		Opp. δ_{asym} S-N-S bending		418m	Opp. δ_{asym} S-N-S bending of $\mathbf{3}^{2+}$
410 (0/1)				414 (3/0)		
		396s	ν_4 AsF_6^-			
354 (0/4)						
				352 (0/14)		
				343 (0/1)		
314 (5/0)						
	288vs		ν_4 SbF_6^-			
				298 (2/0)		
				291 (0/1)		
271 (0/3)						
237(0/1)				249 (0/1)		
204 (0/1)				195 (0/1)		
170 (1/0)				175 (1/0)		
143 (2/0)				149 (1/0)		
102 (0/1)				134 (0/1)		
53 (1/0)				64 (1/0)		

[a] Assignment where made by visualization in Chemcraft [14] (ν = stretching, δ = bending, Asym. = asymmetric, Sym. = symmetric, Inp. = in-plane, Opp = out-of-plane). [b] See Figure S9b for FT-IR spectra. [c] See Figure S14 for FT-IR spectra [d] The –C=O stretching frequencies are scaled by 0.965.[e] See Figure S26b for FT-IR spectra. [f] In Figure S14 we note the presence of $\mathbf{3}^{2+}$ in $\mathbf{3}^{+\bullet}$ prepared according to Equation 7 (Section 1.4.6).

Table S5: Calculated gas phase (B3LYP/6-311++G(d,p) and SO_2 solution (PBE1PBE/6-311G(d) energetics

Compound [a]	Gas Phase (B3LYP/6-311++G(d,p)	Solution PBE1PBE/6-311G(d)		Thermal Correction to Gibbs Free Energies [b]	Gas phase Enthalpy (ΔH) [c] KJ mol^{-1}	Solution Enthalpy (ΔH) [c] KJ mol^{-1}	Solution Gibbs free energies (ΔG) [c] KJ mol^{-1}
	Zero point energies (Hartrees)	Enthalpies (Hartrees)	Gibbs free energy (Hartrees)				
1,4-benzoquinone ($C_6H_4O_2$)	-381.477430	-381.116855	-381.102190	0.055115			
A (Scheme 1)		-1231.718595	-1231.711756		-48 (Eqn. 1a)[a]	-82 (Eqn. 1a)[a]	-47 (Eqn. 1a)[a]
$\mathbf{1}^+$	-1232.401809	-1231.768822	-1231.751612	0.059034	-170 (Eqn. 1b)[a]	-153 (Eqn.1b)[a]	-149 (Eqn. 1b)[a]
$\mathbf{5}^+$	-1231.158945	-1230.514981	-1230.497539	0.035719	24 (Eqn. 2)[a]	-15 (Eqn. 2)[a]	-18 (Eqn. 2)[a]
$\mathbf{7}^{2+}$	-2081.888457	-2081.083783	-2081.063434	0.038937	293 (Eqn.3a)[a]	-17 (Eqn. 3a)[a]	21 (Eqn. 3a)[a]
$\mathbf{8}^{2+}$	-2081.941352	-2081.127652	-2081.107467	0.039454	-139 (Eqn. 3b)[a]	-115 (Eqn. 3b)[a]	-114 (Eqn. 3b)[a]
$\mathbf{3}^{2+}$	-2080.705992	-2079.885445	-2079.865120	0.018510	4 (Eqn. 4)[a]	-46 (Eqn. 4)[a]	-43 (Eqn. 4)[a]
$\mathbf{SNS}^+$	-850.841279	-850.562501	-850.554757	-0.015962			
$\mathbf{NH_4}^+$	-56.870873	-56.953287	-56.946742	0.029829			
$\mathbf{S_8}$	-3185.751246	-3184.514546	-3184.496332	-0.027034			

[a] Based on Equation 1-4 in Scheme 1. [b] Thermal correction from gas phase calculation applied to solution Gibbs free energies. [c] Calculated enthalpies and Gibbs free energies are based on both Scheme 1 and the following proposed reaction: $SNS^+ + 4\ H^+ + 4\ e^- \rightarrow NH_4^+ + ¼S_8$ (Based on Equation 2 and 4 in Scheme 1).

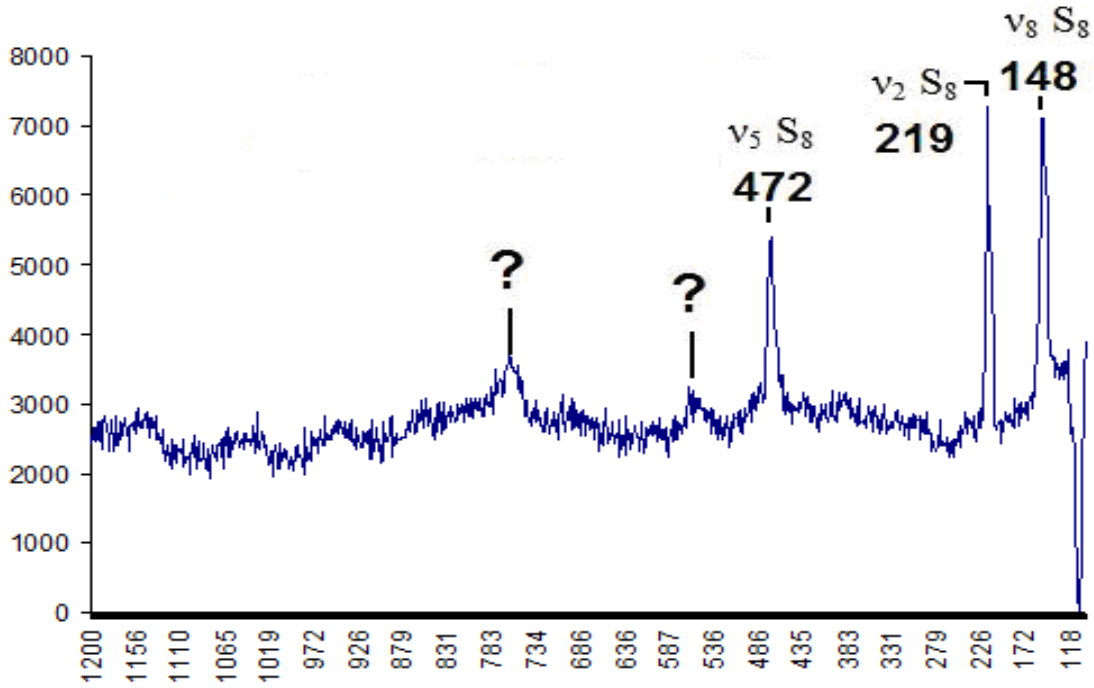

Figure S10: The Raman microscopy (785 nm) of insoluble solid obtained in Section 1.4.5 prepared according to Equation 2-4 in Scheme 1.

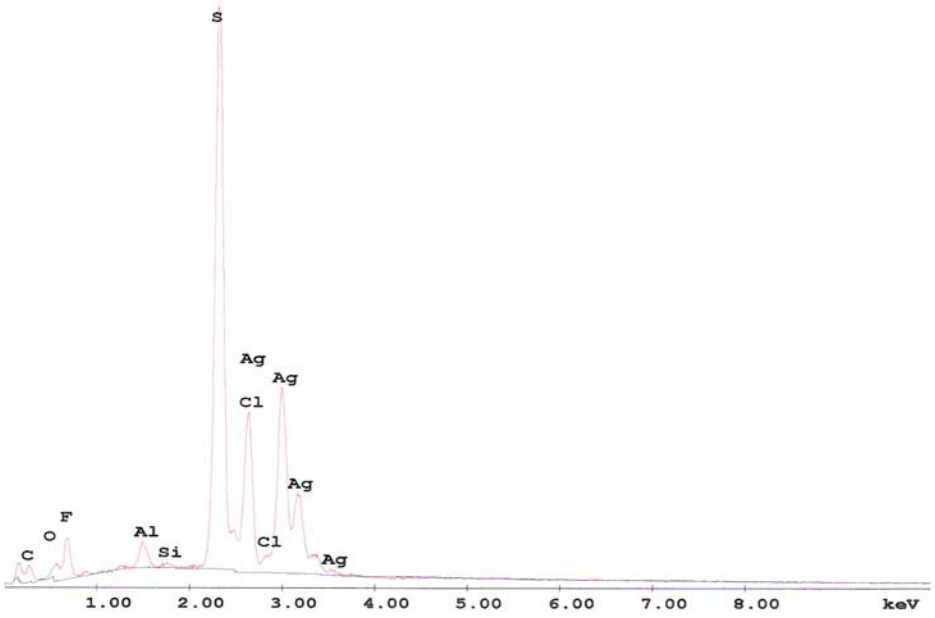

Figure S11: The qualitative microanalysis of the insoluble solid obtained in Section 1.4.5 prepared according to Equation 2 by Scanning Electron Microscopy (SEM).

1.4.5 Purification of $3(SbF_6)_2$ prepared according to Equation 2-4 in Scheme 1 from CH_3CN and CH_2Cl_2

Crude **3**$(SbF_6)_2$ (3.098 g) was added to bulb A of a vessel of Type B (Figure S1b). CH_3CN (13.134 g; ~ 17 ml) was condensed into bulb A. A green-blue solution over a grey insoluble was obtained on warming to ambient temperature. The more soluble fraction was filtered to the bulb B. The volatiles were condensed back to bulb A. The more soluble fraction was filtered to bulb B. The washing was repeated twice more. CH_2Cl_2 (32.510 g; ~ 25 ml) was condensed into bulb B. Upon warming a green solution formed over clear, pale green crystals. The more soluble fraction was filtered to bulb A. A small fraction (~ 2 ml) of the volatiles was condensed back to bulb B containing the pale green crystals. The more soluble fraction was filtered to bulb A. This was repeated twice more. The volatiles were removed under dynamic vacuum. The clear pale green crystals (2.376 g, 3.25 mmol, 62 % yield of **3**$(SbF_6)_2$ based on **1**SbF_6 and Equation 2-4 in Scheme 1) and the solid in bulb A (0.703 g) were collected in the drybox. The IR of the pale green crystals from bulb B was obtained as a Nujol mull on CsI plates (Figure S9b) and was consistent with **3**$(SbF_6)_2$ by comparison to Figure S9a and the calculated frequencies and intensities in Table S4.
The solid from bulb A was washed with water on a Buchner funnel, followed by acetone and air dried for 24 hours before performing Raman microscopy (Figure S10) and qualitative EDX microanalysis by scanning electron microscopy (SEM) in Figure S11. The sample was mounted on carbon tape and the results showed the presence of mainly S_8 and AgCl (Some AgCl may still be present in $SNSSbF_6$ even after purification)[20] in Figure S11.
Elemental analysis Found C 9.84%, N 4.16%, S 17.07%, < H 0.5%, F 26.08%, Sb 31.9%; Calculated based on **3**$(SbF_6)_2$: C 9.85%, N 3.83%, S 17.53%, H 0%, F 31.95%, Sb 33.27%.

Comments:

1) We note the good agreement for C, N and S while the F analysis obtain from Galbraith Laboratories have been inconsistent, however the Sb analyses have been satisfactory (See also section 1.4.4).

1.4.6 Reduction of $3(SbF_6)_2$ with CsI in SO_2 according to Equation 4

3$(SbF_6)_2$ (3.098 g, 4.24 mmol) and CsI (1.067 g, 4.15 mmol) were added to bulb A of a vessel of Type B (Figure S1b) with an EPR tube attached directly via ¼ inch Pyrex tube. SO_2 (15.734 g; ~ 11 ml) was condensed onto the mixture in bulb A. A green-blue solution over a white insoluble (c.f. $CsSbF_6$) was obtained upon warming to ambient temperature. The more soluble fraction was filtered to bulb B and the volatiles condensed back to bulb A. The more soluble fraction in bulb A was filtered into bulb B. This was repeated two more times. The more soluble fractions collected in bulb B were filtered to the attached EPR tube and the ambient temperature X-band EPR obtained (See Figure 2a, main text of Chemical Communication) which is consistent with the calculated SOMO of $\mathbf{3}^{+\bullet}$ (Figure S12b). A comparison of the experimental and calculated hyperfine coupling constants (*a*) for $\mathbf{3}^{+\bullet}$ and related 1,3,2-dithiazolyl are given in Table S6. The volatiles were removed under dynamic vacuum. The pale green solid in bulb B (2.376 g) and the white insoluble solid in bulb A (0.703 g) were collected in the drybox. The IR of the pale green solid was obtained as a Nujol mull on KBr plates (Figure S13) and indicated a

mixture of **3**$(SbF_6)_2$ and several peaks that we tentatively assign to **3**SbF_6 based on the comparison to the calculated IR frequencies and intensities given in Table S4.

Equation 7:

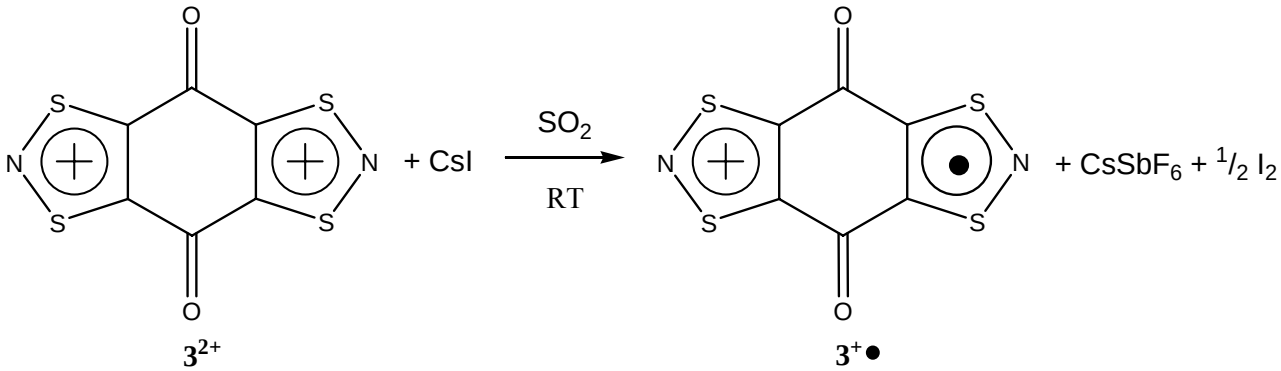

$\mathbf{3}^{2+}$ $\mathbf{3}^{+\bullet}$

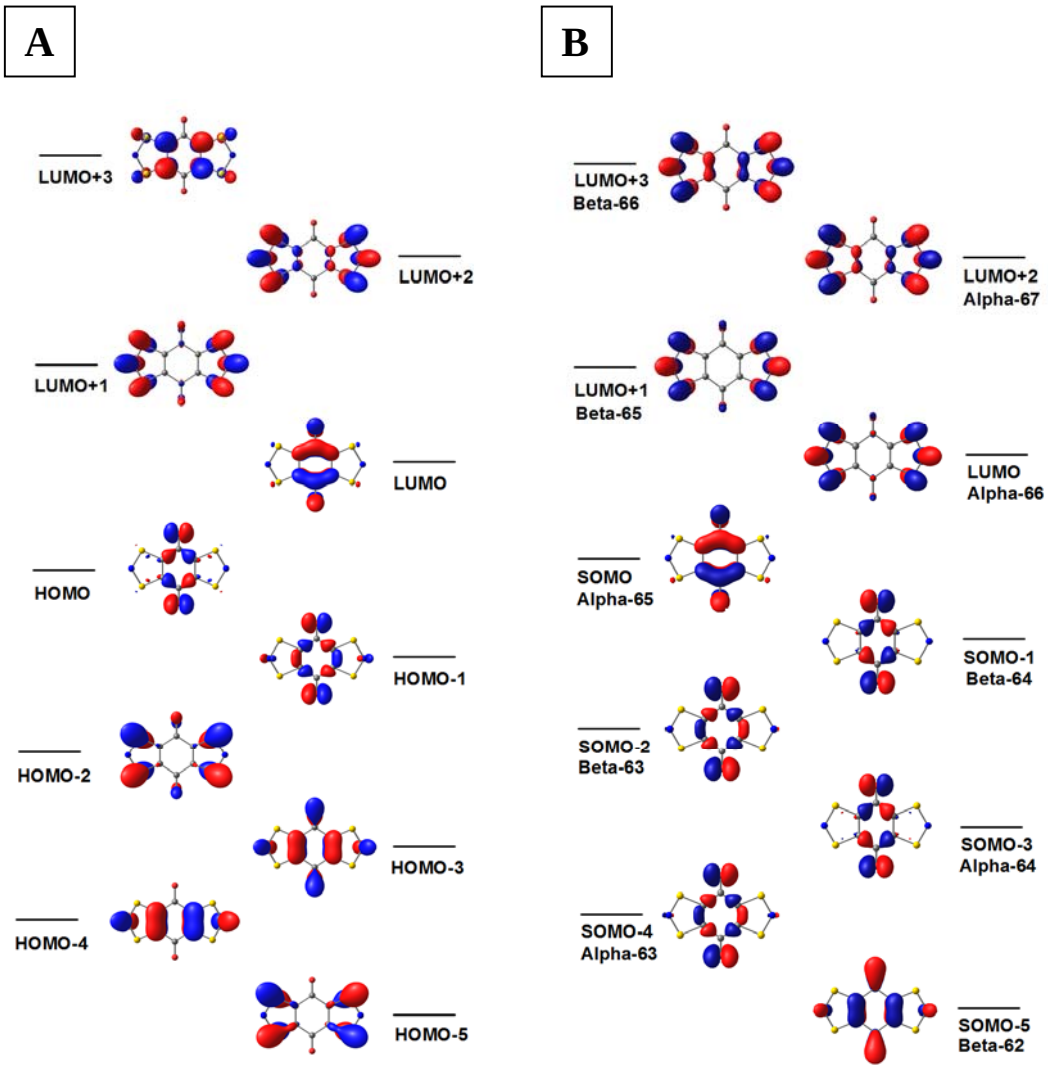

Figure S12: Selected frontier molecular orbitals of a) $\mathbf{3}^{2+}$ and b) $\mathbf{3}^{+\bullet}$ calculated at the B3LYP/6-311++G(d,p) level of theory.

Discussion of Figure S12: We note the SOMO (alpha-65) in Figure S12b of $\mathbf{3}^{+\bullet}$ (c.f. LUMO in Figure S12a of $\mathbf{3}^{2+}$) is based largely on the 1,4-benzoquinodal ring and oxygen, consistent with the observed EPR spectrum (Figure 2, main text of the Chemical Communication). This contrasts $\mathbf{4}^{+\bullet}$ which is a typical 1,3,2-dithiazolyl radical with little delocalization of spin density on to the bridging benzo- ring.[21] Furthermore, the LUMO (alpha-66, Figure S12b) is largely located on the 1,3,2-dithiazolyl ring which suggests $\mathbf{3}^{\bullet\bullet}$ should be a diradical similar to that of $\mathbf{4}^{\bullet\bullet}$.[22] We also note the calculated hyperfine a_N coupling (c.f. 0.108 mT, see Table S6) of $\mathbf{3}^{+\bullet}$ is consistent with the lack of electron density on the adjacent sulphur atoms depicted in the SOMO (alpha-65, Figure S12b). In addition, the π-bonding HOMO-3 and HOMO-4 in Figure S12a help rationalize the similarity of the bond lengths in the 1,4-benzoquinodal bridge in $\mathbf{3}^{2+}$ (Table S3) in comparison to 1,4-benzoquinone (Table S8; c.f. C=O 1.200 Å and 1.19 Å in $\mathbf{3}^{2+}$ and 1,4-benzoquinone, respectively) while the anti-bonding character of the HOMO and HOMO-1 may account for the slight lengthening of the C=C bonding length (c.f. C2-C3 1.371 Å and 1.30 Å in $\mathbf{3}^{2+}$ and 1,4-benzoquinone, respectively).

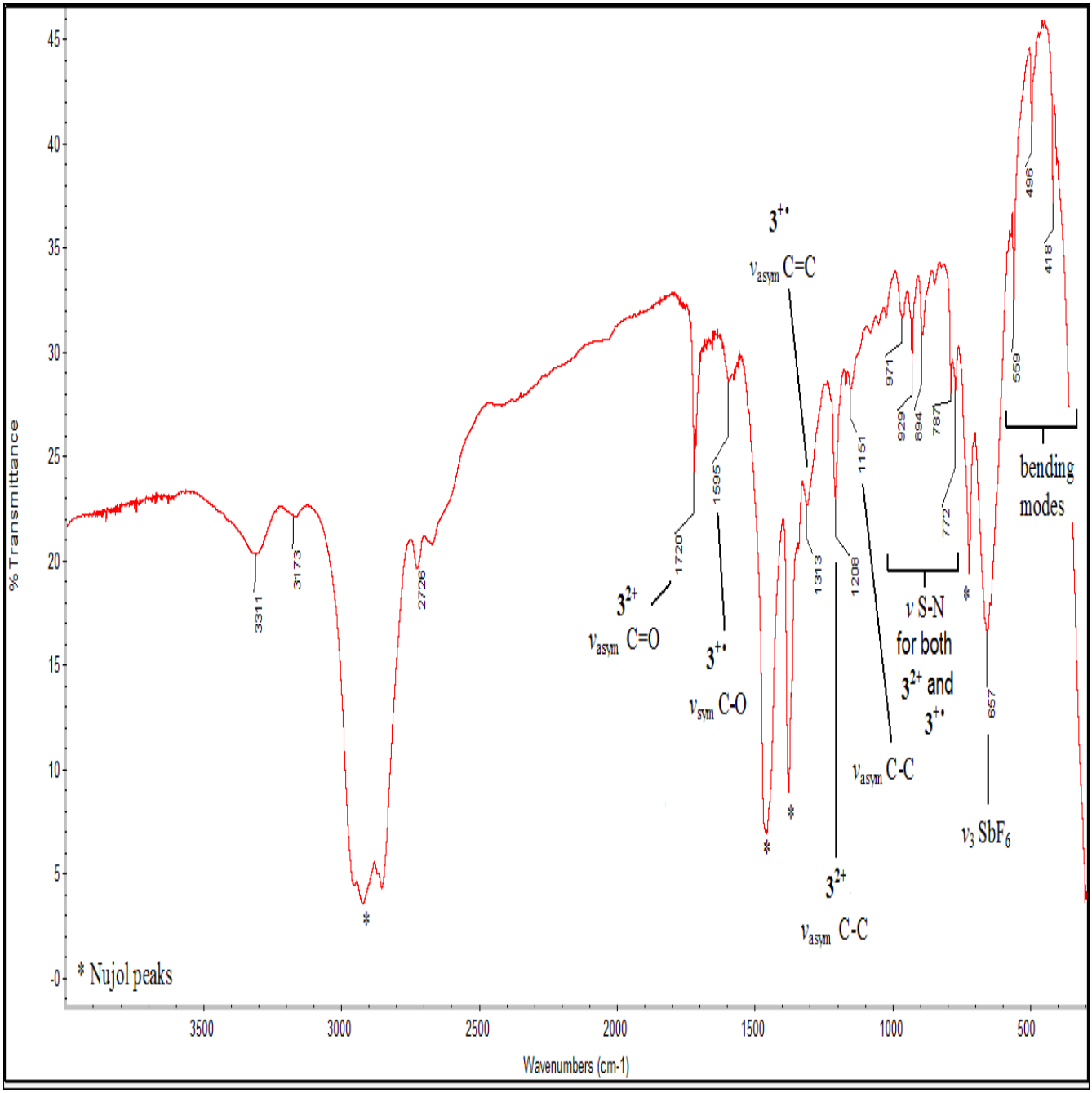

Figure S13: FT-IR of the recovered pale green solid from the reduction of **3**$(SbF_6)_2$ with CsI in SO_2 (32 scans, 2 cm^{-1} resolution) according to Equation 7. See Table S4 for comparison of experimental and calculated IR frequencies and tentative assignments (Note the tentative assignments: ν = stretch, δ =bending, asym. = asymmetric and sym = symmetric):

Table S6: Comparison of calculated (B1LYP//EPR-II/6-31G(2d,p)) and experimental hyperfine coupling constants of **1**$^{\bullet}$, **5**$^{\bullet}$, **3**$^{+\bullet}$ and the related benzofused 1,3,2-dithiazolyl **9** (Atom labelling given below):

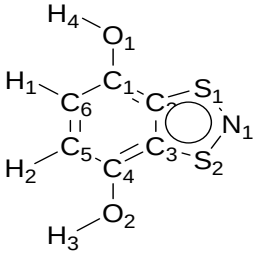

1 $^{\bullet}$

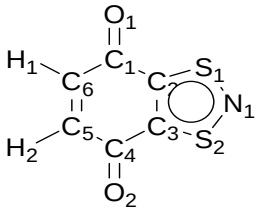

5 $^{\bullet}$

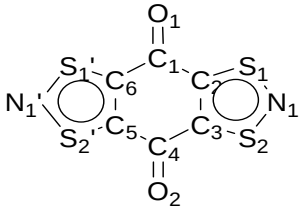

$3^{+\bullet}$

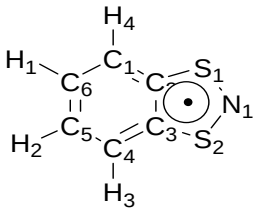

9

	1$^{\bullet}$			**5**$^{\bullet}$			**3**$^{+\bullet}$			**9**	
	Calc.	**Exp.**[15]		**Calc.**	**Exp.** [a]		**Calc.**	**Exp.** [a]		**Calc.**	**Exp.**[23]
	a (mT)			*a* (mT)			*a* (mT)			*a* (mT)	
g-value		2.0046			2.005			2.007			2.008
O1	0.0072			-0.0619			-0.8456				
O2	0.0072			-0.0619			-0.8456				
C1	0.0183			-0.0647			-0.5903			0.1229	
C2	-0.1637			-0.1672			0.1495			-0.1723	
C3	-0.1637			-0.1672			0.1495			-0.1723	
C4	0.0183			-0.0647			-0.5903			0.1229	
C5	0.0090			0.0069			0.1495			0.0076	
C6	0.0090			0.0069			0.1495			0.0076	
H1	-0.0504			-0.0291						-0.0919 [b]	
H2	-0.0504			-0.0291						-0.0919 [b]	
H3	-0.0058									-0.0706 [b]	
H4	-0.0058									-0.0706 [b]	
S1	0.1883			0.2261			0.0447			0.2246	
S2	0.1883			0.2261			0.0447			0.2246	
N1	1.1188	1.073		1.0633	1.013		-0.1080			1.1144	1.12

[a] This work. [b] Hyperfine coupling to the H atoms have not been experimentally observed.

1.4.7 *In situ* multinuclear NMR of the reaction of $SNSSbF_6$ and with two equivalents of 1,4-benzoquinone ($C_6H_4O_2$) in liquid SO_2 designed to give $5SbF_6$ and 1,4-hydroquinone ($C_6H_4(OH)_2$) according to Equation 8b

1,4-benzoquinone ($C_6H_4O_2$, 0.218 g, 2.02 mmol) and $SNSSbF_6$ (0.314 g, 1.00 mmol) were loaded in separate bulbs of a vessel of Type B (Figure S1b) with a 10 mm NMR tube directly attached via a ¼ inch Pyrex tube. SO_2 (9.893 g) was condensed onto both reactants to produce two yellow solutions. The two yellow solutions were mixed producing a forest green solution after stirring for 1 hr. After continuous stirring for 12 hrs a deep blue solution was obtained. A small portion (5.109 g) of the solution was poured into the NMR tube and flame sealed. The multinuclear NMR (^{1}H, ^{13}C, ^{14}N) was followed over time (See Figure S14, S15 and S16). The remaining solution was slowly concentrated over a temperature gradient of 0-5 ^{o}C yielding blue-black solid. The volatiles were removed under dynamic vacuum and the solid collected (0.250 g, 47 % recovered of $\mathbf{1}SbF_6 \bullet C_6H_4O_2$ based on $SNSSbF_6$ and Equation 8a) in the drybox. Small needles were mechanically separated from the solid and the X-ray structure determined (See Figure S17 and Table S7). The IR was obtained as a Nujol mull on CsI plates (Figure S18) and assigned as the lattice inclusion compound $\mathbf{1}SbF_6 \bullet C_6H_4O_2$. The IR (Figure S18) of $\mathbf{1}SbF_6 \bullet C_6H_4O_2$ was consistent with the presence of 1,4-benzoquinone

(c.f. 1654m, br cm^{-1} in Figure S18) and is comparable to Figure S3a which contains a small quantity of 1,4-benzoquinone. However, three frequencies (cm^{-1}) 1095, 1022 and 804 are clearly visible in Figure S17 which are not observed in purified **1**SbF_6 (Figure S3b). These are tentatively assigned to C-H bending modes and out-of-plane ring bending modes on comparison to the calculated IR of **1**MF_6, **1**SbF_6•$C_6H_4O_2$ and 1,4-benzoquinone ($C_6H_4O_2$) given in Table S8.

The multinuclear NMR (^1H, ^{13}C, ^{14}N) clearly exhibits two unassociated species in solution (see Table S2 for comparison of experimental and calculated multinuclear NMR).

^{1}H-NMR: The ^{1}H-NMR (Figure S14) indicated the presence of 1,4-bezoquinone (C-H, δ 6.8), **1**SbF_6 (C-H δ 8.0 and O-H δ 7.5) and NH_4^+ (1:1:1 triplet centered at δ 6.0, $J_{N\text{-}H}$ = 54 Hz).

^{13}C-NMR: The decoupled ^{13}C-NMR (Figure S15) is also consistent with the assigned ^{1}H-NMR (Figure S14). The 1,4-benzoquinone δ 136.9 (C-H) and δ 188.7 (C=O) and **1**SbF_6 δ 154.5 (C-S), δ 146.3 (C-O) and δ 120.2 (C-H) (c.f. δ 154.8, 146.5, 119.5 for **1**SbF_6)[15] were observed in the ^{13}C-NMR and two small unassigned peaks δ 139.3 and δ 136.1.

^{14}N-NMR: The ^{14}N-NMR (Figure S16) δ -5.7 is assigned to **1**SbF_6 (c.f. δ -7.4)[15] and a poorly resolved pentet centered at δ -361.3 for NH_4^+ ($J_{N\text{-}H}$ = 54 Hz).

Comments:
1) The oxidation of **1**SbF_6 by 1,4-benzoquinone designed to give **5**SbF_6 based on Equation 8b was calculated (B3LYP/6-311++G**) to be unfavourable in the gas phase by 67 KJ mol^{-1}.

2) The X-ray crystal structure determination is definitive evidence of the 1:1 lattice inclusion complex **1**SbF_6•$C_6H_4O_2$ (See Figure S17 and Table S7 for comparison of experimental and calculated bond lengths (Å) and angles (^{o})). We note that the major interaction between $\mathbf{1}^+$ and 1,4-benzoquinone is the electostatic $S^{\delta+}$---$O^{\delta-}$ of 3.039(1) Å (Figure S17). The norbornene-like 1,4-dithia-7-azabicyclo[2.2.1]heptane derivative (Equation 8c) was not obtained[24], which is unfavourable in the gas phase (B3LYP/6-31G*) by 55 KJ mol^{-1}.

Equation 8a:

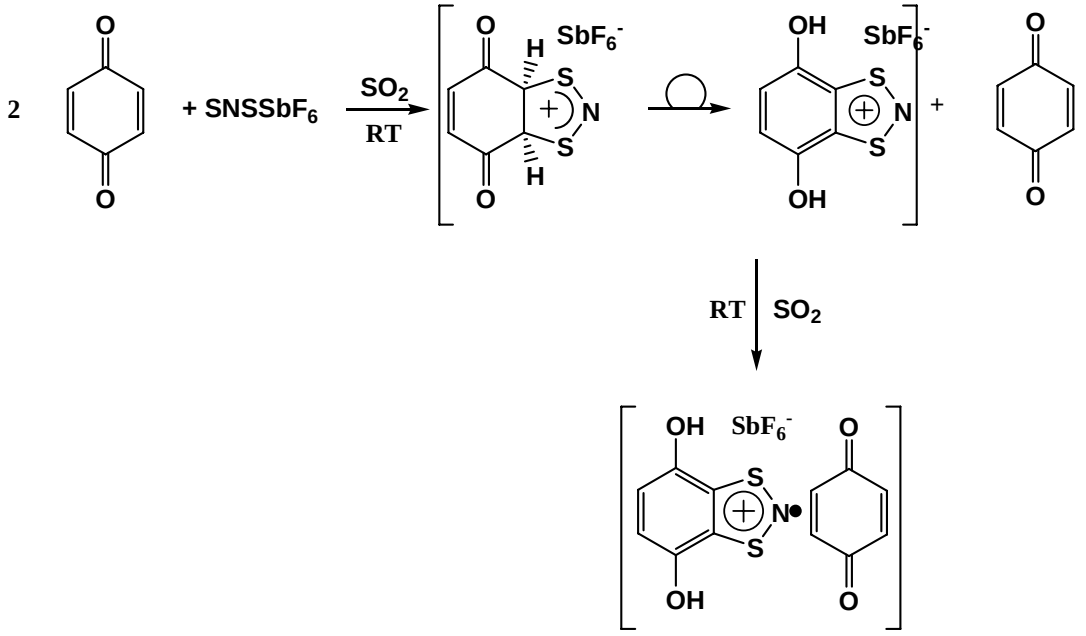

Equation 8b:

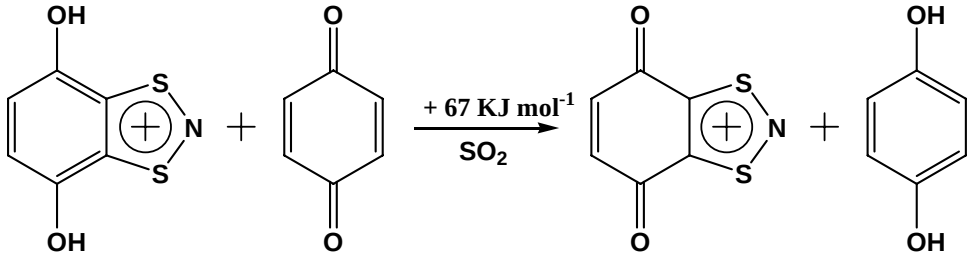

1^+ 1,4-benzoquinone ($C_6H_4O_2$) 5^+ 1,4-hydroquinone

Equation 8c:

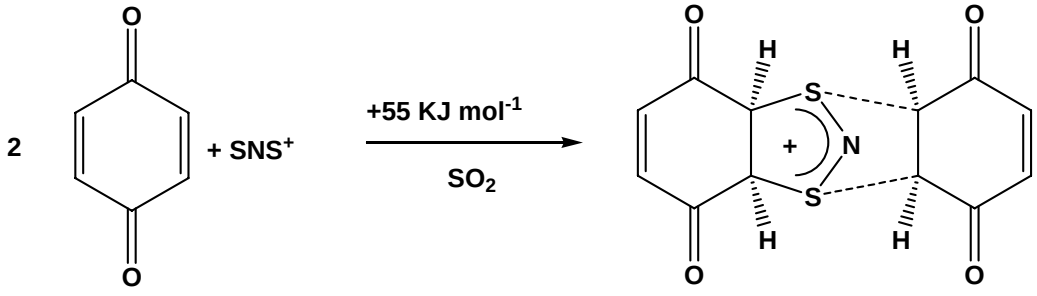

1,4-benzoquinone ($C_6H_4O_2$)

1,4-dithia-7-azabicyclo[2.2.1]heptane derivative

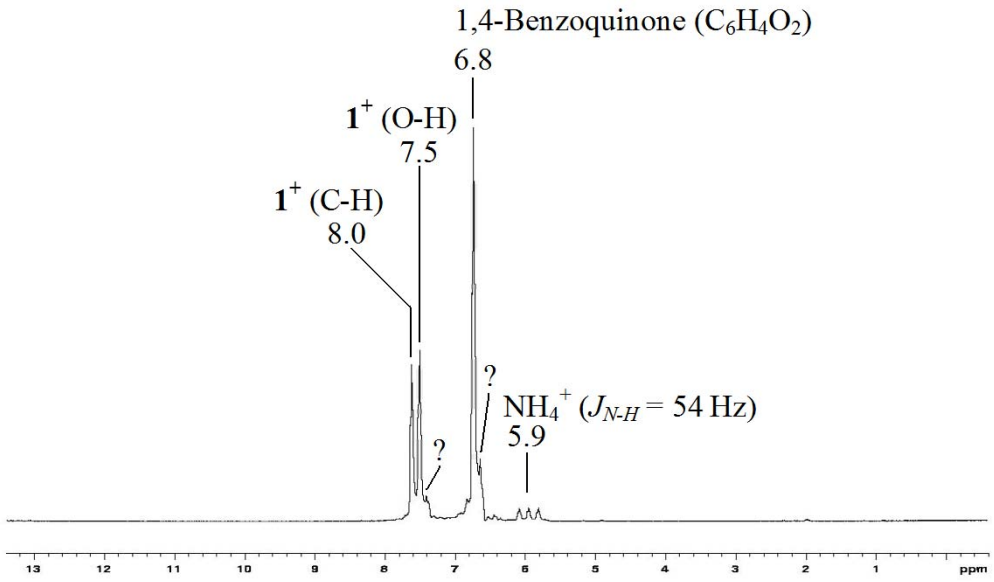

Figure S14: ^{1}H-NMR of the *in situ* NMR of the reaction of $SNSSbF_6$ and with two equivalents of 1,4-benzoquinone in liquid SO_2 at 25 ^oC.

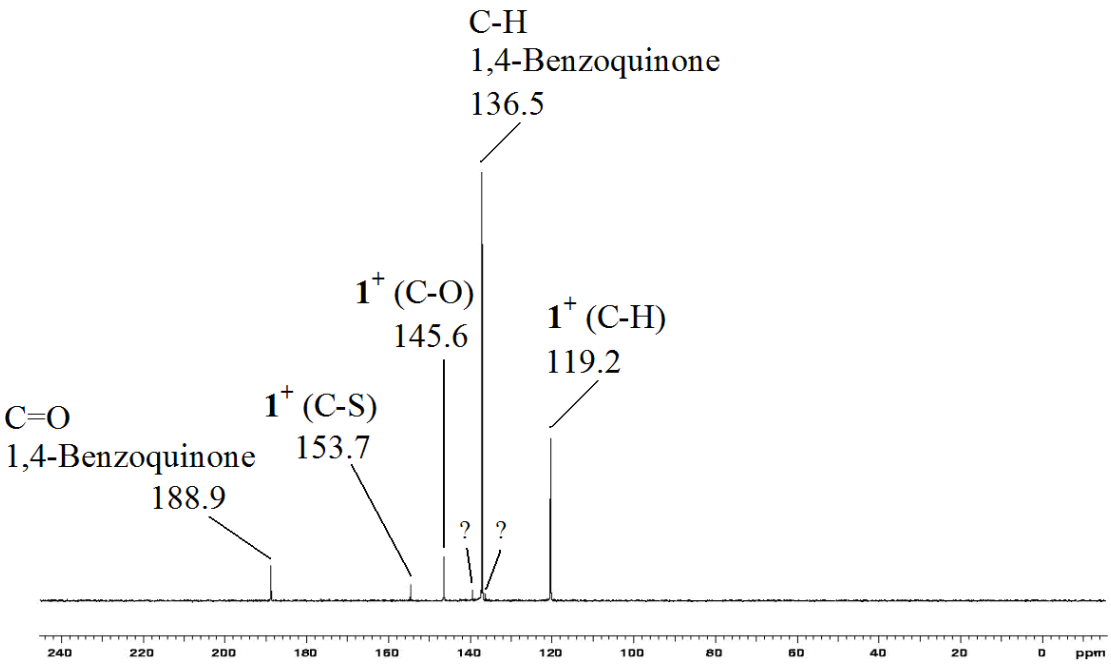

Figure S15: ^{13}C-NMR of the *in situ* NMR of the reaction of $SNSSbF_6$ and with two equivalents of 1,4-benzoquinone in liquid SO_2 at 25 ^oC.

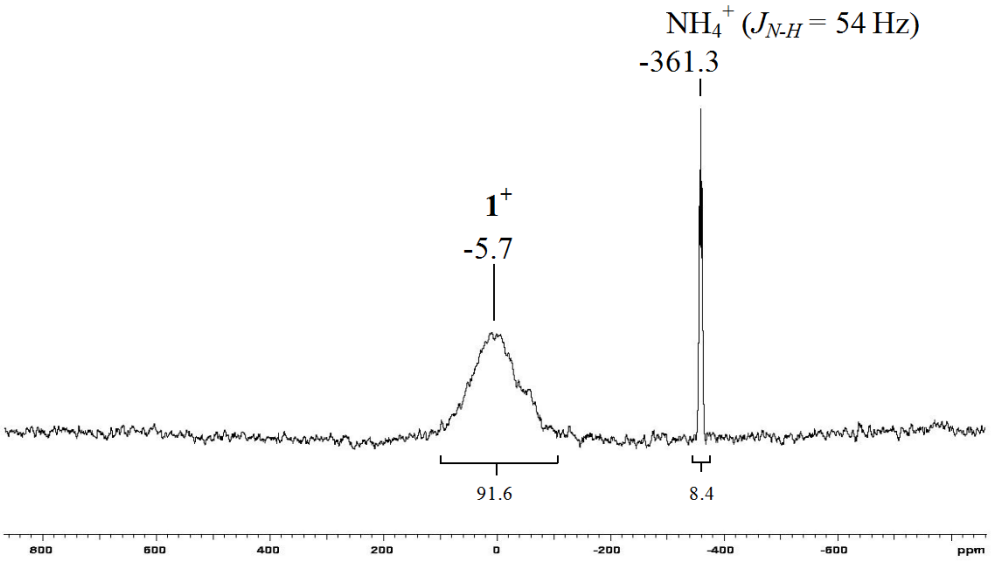

Figure S16: ^{14}N-NMR of the *in situ* NMR of the reaction of $SNSSbF_6$ and with two equivalents of 1,4-benzoquinone in liquid SO_2 at 25 ^{o}C.

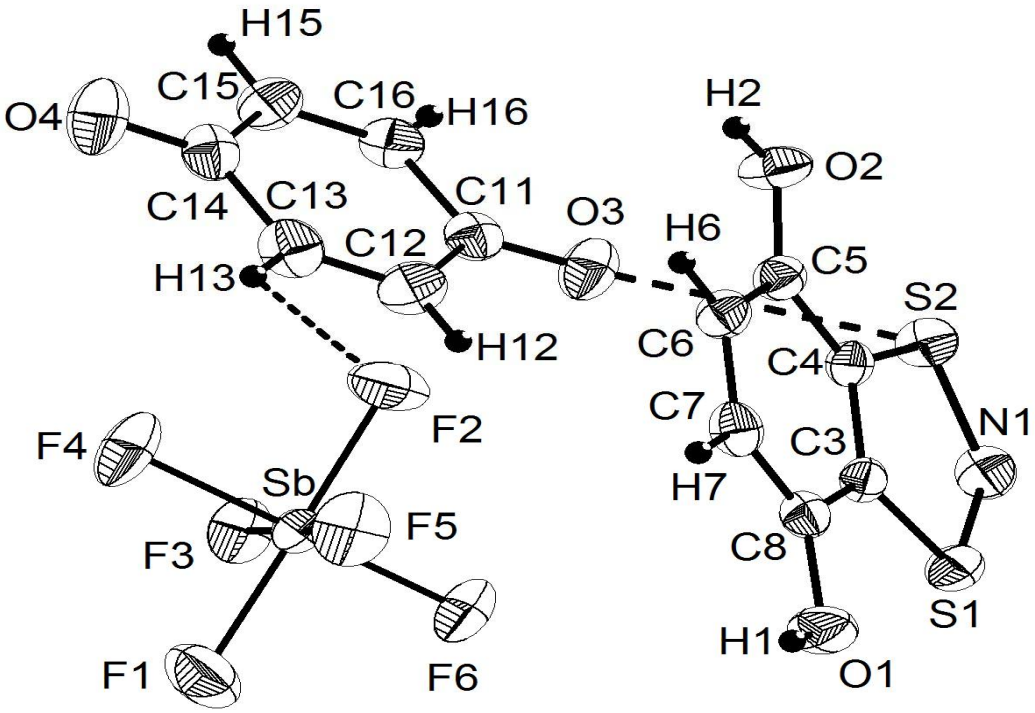

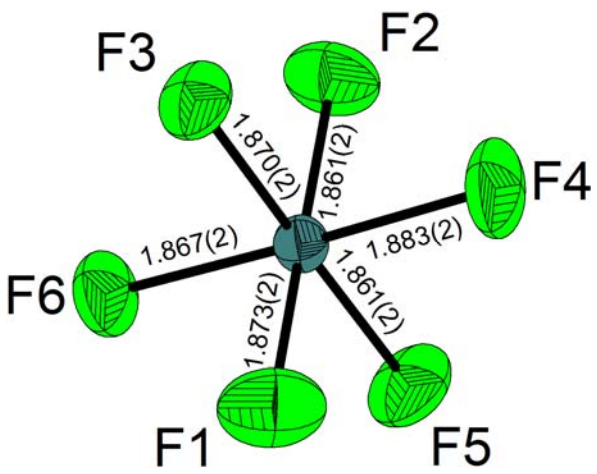

F1-Sb1-F2 = 179.98 (8), F1-Sb1-F3 = 89.85(8), F1-Sb1-F4 = 89.56(8), F1-Sb1-F5 = 90.20(8), F1-Sb1-F6 = 90.84(8), F2-Sb1-F3 = 89.49(8), F2-Sb1-F4 = 89.63(8), F2-Sb1-F5 = 90.44(8), F2-Sb1-F6 = 89.97(8), F3-Sb1-F4 = 88.42(8), F3-Sb1-F5 = 178.98(7), F3-Sb1-F6 = 89.95(7), F4-Sb1-F5 = 90.55(8), F4-Sb1-F6 = 178.32(8), F5-Sb1-F6 = 91.08(7).

Figure S17: A representative view of the single crystal X-ray structure determination of **1**SbF_6•$C_6H_4O_2$ and the SbF_6^- anions. Thermal ellipsoids drawn at 50 % probability and H atoms shown as black spheres (0.145 Å diameter). Hydrogen bonds and S---O interactions shown as dashed lines. Experimental and calculated bond distances (Å) and angles (^{o}) are compared in Table S7.

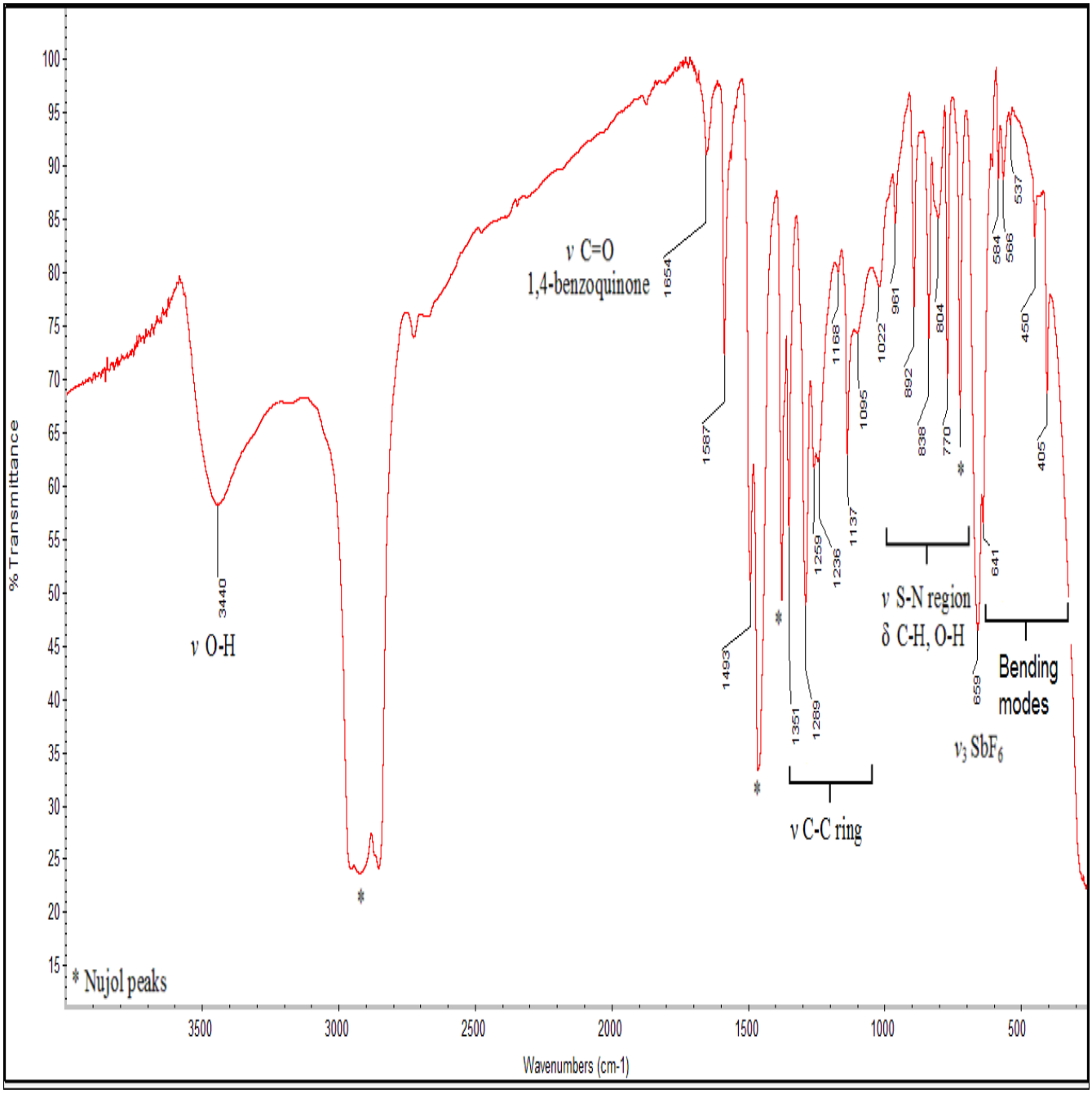

Figure S18: FT-IR of reaction of two equivalents of 1,4-benzoquinone ($C_6H_4O_2$) with $SNSSbF_6$ to giving **1**SbF_6•$C_6H_4O_2$ as Nujol mull on KBr plates (32 scans, 2 cm^{-1} resolution). See Table S8 for comparison of experimental and calculated IR frequencies and tentative assignments (Note the tentative assignments: ν = stretch, δ =bending, asym. = asymmetric and sym = symmetric):

Table S7: Comparison of calculated (B3LYP/6-311++G(d,p)) bond lengths (Å) and angles (°) of **1**SbF_6 and 1,4-benzoquinone ($C_6H_4O_2$) and experimental bond lengths (Å) and angles (°) for **1**SbF_6•$C_6H_4O_2$:

Bond	**1**SbF_6•$C_6H_4O_2$ [a]	Calc. $\mathbf{1}^+$	Calc.[b] **1,4-benzoquinone ($\mathbf{C_6H_4O_2}$)**
Bond Length (Å)			
H1-O1	0.638(29)	0.965	
O1-C8	1.350(3)	1.351	
C8-C3	1.403(4)	1.406	
C3-C4	1.399(3)	1.413	
C4-C5	1.404(3)	1.406	
O2-C5	1.352(3)	1.351	
H2-O2	0.718(37)	0.965	
C5-C6	1.373(4)	1.387	
C6-C7	1.394(4)	1.407	
H6-C6	0.877(26)	1.085	
C7-C8	1.369(4)	1.387	
H7-C7	0.891(29)	1.085	
C3-S1	1.707(3)	1.736	
S1-N1	1.600(2)	1.615	
S2-N1	1.594(2)	1.615	
C4-S2	1.703(3)	1.736	
C11-C12	1.470(4)		1.486
O3-C11	1.222(3)		1.220
C12-C13	1.316(4)		1.340
H12-C12	0.827(34)		1.084
C13-C14	1.472(4)		1.486
H13-C13	0.926(28)		1.084
C14-C15	1.467(4)		1.486
O4-C14	1.219(3)		1.220
C15-C16	1.323(4)		1.340
H15-C15	0.904(27)		1.084
C16-C11	1.467(4)		1.486
H16-C16	0.882(28)		1.084
Bond Angles (°)			
H1-O1-C8	110.63(241)	112.48	
O1-C8-C3	116.17(23)	116.20	
O1-C8-C7	126.83(24)	126.72	
C8-C3-C4	121.08(23)	121.13	
C3-C4-C5	121.11(23)	121.13	
C4-C5-C6	116.67(23)	117.09	
O2-C5-C4	115.85(21)	116.20	
O2-C5-C6	127.48(23)	126.72	
H2-O2-C5	110.89(299)	112.48	
C5-C6-C7	122.20(24)	121.78	
C6-C7-C8	121.93(24)	121.78	
H6-C6-C5	119.24(173)	119.56	
H6-C6-C7	118.41(171)	118.67	
C7-C8-C3	117.00(24)	117.09	
H7-C7-C8	115.93(176)	119.56	
H7-C7-C6	122.14(176)	118.67	
C3-S1-N1	99.31(12)	98.43	
C3-C4-S2	112.92(18)	112.84	

S1-N1-S2	116.13(14)	117.47	
C4-S2-N1	99.31(12)	98.43	
C4-C3-S1	112.33(19)	112.84	
C11-C12-C13	121.09(25)		121.33
O3-C11-C12	120.95(24)		121.33
O3-C11-C16	121.46(24)		121.33
C12-C13-C14	121.59(25)		121.33
H12-C12-C11	117.56(207)		115.93
H12-C12-C13	121.33(219)		122.74
C13-C14-C15	117.09(23)		117.34
H13-C13-C12	122.42(170)		122.74
H13-C13-C14	115.94(167)		115.93
C14-C15-C16	121.54(25)		121.33
O4-C14-C13	121.42(24)		121.33
O4-C14-C15	121.48(24)		121.33
C15-C16-C11	121.05(24)		121.33
H15-C15-C14	117.63(179)		115.93
H15-C15-C16	120.79(171)		122.74
C16-C11-C12	117.58(22)		117.34
H16-C16-C15	123.43(178)		122.74
H16-C16-C11	115.52(175)		115.93

[a] See Table S1 for X-ray crystallographic details in Section 1.2
[b] Calculated at the B3LYP and 6-311++G(d,p) level of theory. See Table S9 for comparison to experimental bond length (Å) and angles (^{o})

Table S8: Comparison of calculated (B3LYP/6-311++G(d,p)) and experimental IR frequencies for **1**MF_6 (M = As, Sb), **1**SbF_6•$C_6H_4O_2$ and 1,4-benzoquinone ($C_6H_4O_2$):

1MF_6 (M = As, Sb)			**1**SbF_6•$C_6H_4O_2$	1,4-benzoquinone $C_6H_4O_2$	Tentative Assignments [a]
IR (Calc.) [e]	Observed IR (**1**SbF_6) [b]	Observed IR (**1**AsF_6) [c]	Observed IR [d]	IR (Calc.) [e]	
3817 (48)					
3815 (86)	3449vs,br	3481vs,br	3440vs, br		ν_{sym} OH
3189 (1)					
3178 (1)	3169s,br	3164s,br			ν_{asym} OH
				3195 (0)	
				3192 (1)	
				3176 (1)	
				3176 (1)	
				1668 (1)	
			1654m	1667 (100)	ν_{asym} C=O
1628 (2)					
				1616 (0)	
1609 (21)	1587m	1586m	1587m		Inp. νC-C + ν_{asym}C-O
				1584 (4)	
1515 (100)	1492s,sh	1489s,sh	1493s,sh		Inp. νC-C + ν_{sym}C-O
1419 (0)					
				1393 (0)	
				1383 (1)	
1369 (24)	1351s,sh	1350s,sh	1351s,sh		Inp. νC-C+ δ_{sym}C-H
1319 (92)	1289s	1286s	1289s		Inp. νC-C + δ_{asym}C-H bending
				1313 (17)	
1305 (16)					
			1259m,sh	1232 (0)	Inp. ν_{asym}C-C ring + δ_{asym}C-H bending
1223 (88)	1243s,br	1236s,br	1236m,sh		δ_{asym}O-H
1186 (4)	1171w	1168w	1168w		δ_{sym}C-H+ δ_{sym}OH
				1167 (0)	
1144 (2)					
1134 (27)	1137m	1136m	1137m		δ_{asym}C-H+ δ_{asym}OH
			1095m,sh	1083 (10)	
			1022 m,br	1011 (0)	
				1004 (0)	
982 (0)					
954 (7)	961w	963w	961w		Opp. νC-C + δ_{sym}C-H bending
				947 (4)	
934 (0)					
				901 (17)	
892 (15)	892m	891m	892m		ν_{asym} S-N
839 (17)	838m	836m	838m		

			804m	780 (0)	
				769 (0)	Opp. δ_{sym}C-H
764 (14)	771m	773m	770m		ν_{sym} S-N
				754 (0)	
				752 (0)	
727 (12)					
		698vs,br			ν_3 AsF_6^-
	659vs,br		659vs,br		ν_3 SbF_6^-
		673s,sh			?
	635s,sh		642s,sh		?
		603w			?
				602 (0)	
589 (0)					
586 (2)	584w	580w	584w		δ CSNSC ring
584 (0)					
564 (5)	566w	564w	566w		Inp. δ ring
536 (0)		538w	537w		Inp. δ ring
				513 (1)	
				458 (0)	
				455 (0)	
449 (2)	450w	450w	450w		Inp. δ ring
				413 (5)	
412 (5)	405m		405m		Opp. δ ring
406 (0)					
		393vs			ν_4 AsF_6^-
395 (0)					
335 (0)				332 (0)	
299 (85)					
287 (0)					
263 (0)					
202 (2)				212 (0)	
183 (1)					
136 (2)					
120 (0)					
				90 (3)	

[a] Assignment where made by visualization in Chemcraft [14] (ν = stretching, δ = bending, Asym. = asymmetric, Sym. = symmetric, Inp. = in-plane, Opp = out-of-plane). [b] See Figure S3b for FT-IR spectra. [c] See Figure S2b for FT-IR spectra [d] See Figure S18 for FT-IR spectra [e] Calculated at the B3LYP/6-311++G(d,p) level of theory.

Table S9: Comparison of experimental[25] and calculated (B3LYP/6-311++G(d,p)) bond lengths (Å) and angles (°) of 1,4-Benzoquinone ($C_6H_4O_2$) (Atom labelling is given to right):

	1,4-benzoquinone: $C_6H_4O_2$ (X-ray) [25]	1,4-benzoquinone: $C_6H_4O_2$ (Calc.)
Bond Length (Å)		
O1-C1	1.222(8)	1.220
C1-C2	1.477(6)	1.486
C2-C3	1.322(8)	1.340
Bond Angle (°)		
O1-C1-C2	121.06(27)	121.33
C1-C2-C3	121.06(27)	121.33
C2-C1-C2'	117.48(37)	117.34

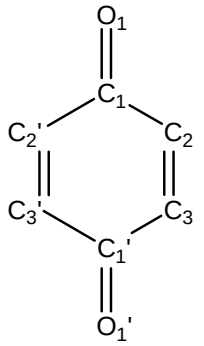

1.4.8 Oxidation of $1AsF_6$ with three equivalents of AsF_5 in the presence of NEt_3 leading to $5AsF_6$ according to Equation 5

Purified **1**AsF_6 (1.097 g, 2.93 mmol) was added in bulb A of a vessel of Type B (Figure S1b). NEt_3 (1 ml, 7.17 mmol) and CH_2Cl_2 (15 ml) were syringed into bulb B in the drybox and degassed by three freeze-pump-thaw cycles. SO_2 (10.314 g) and AsF_5 (1.536 g, 9.04 mmol) were condensed into bulb A consecutively. Upon warming a rapid color change from blue to dark purple was observed and the solution was stirred for 2-5 min. The solution in bulb B was quickly poured into bulb A. Immediately a brown precipitate under an orange-brown solution was obtained. The more soluble fraction was filtered to bulb B and the volatiles removed under dynamic vacuum. Fresh SO_2 (4.378 g; ~3 ml) and CH_2Cl_2 (16.689 g; ~ 13 ml) were condensed into bulb A. A brown solution over a dark insoluble was obtained on warming and the more soluble fraction was filtered to bulb B. The volatiles were condensed back into bulb A and the solid washed and the more soluble fraction filtered to bulb B. The washing was repeated twice more to give a dark purple solid in bulb A. The volatiles were removed and a dark brown solid was obtained in bulb B. The dark purple solid in bulb A (0.973 g, 89 % yield based on **1**AsF_6 and Equation 5) and the brown solid in bulb B (0.103 g) were collected in the drybox. The IR of the purple solid in bulb A was obtained as a Nujol mull on CsI plates (Figure S19) and was consistent with **5**AsF_6 based on comparison of the experimental and calculated IR frequencies given in Table S10.

Comments:

1) We note the absence of the very strong, broad ν O-H (c.f. 3450 cm^{-1} in Figure S2b) and a strong ν C-O (c.f. 1586 cm^{-1} in Figure S2b) and the appearance of a new frequency at 1688 cm^{-1} (Figure S19) assigned to the ν C=O of **5**AsF_6. Furthermore, we note the difference of Figure S19 compared to Figure S2b between 1500-1000 cm (ν C-C and δ C-H region) is attributed to the conversion of the benzonoid (**1**$^+$) to the quinodal (**5**$^+$**)** ring.

Equation 5:

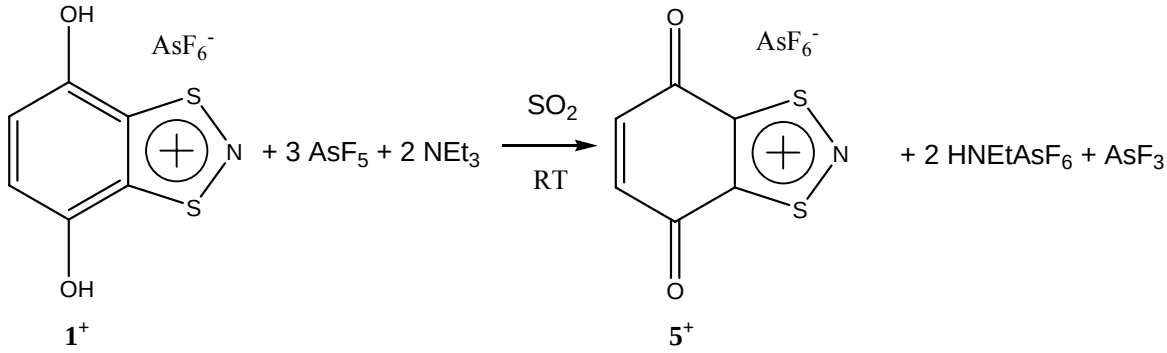

1^{+} **5**$^{+}$

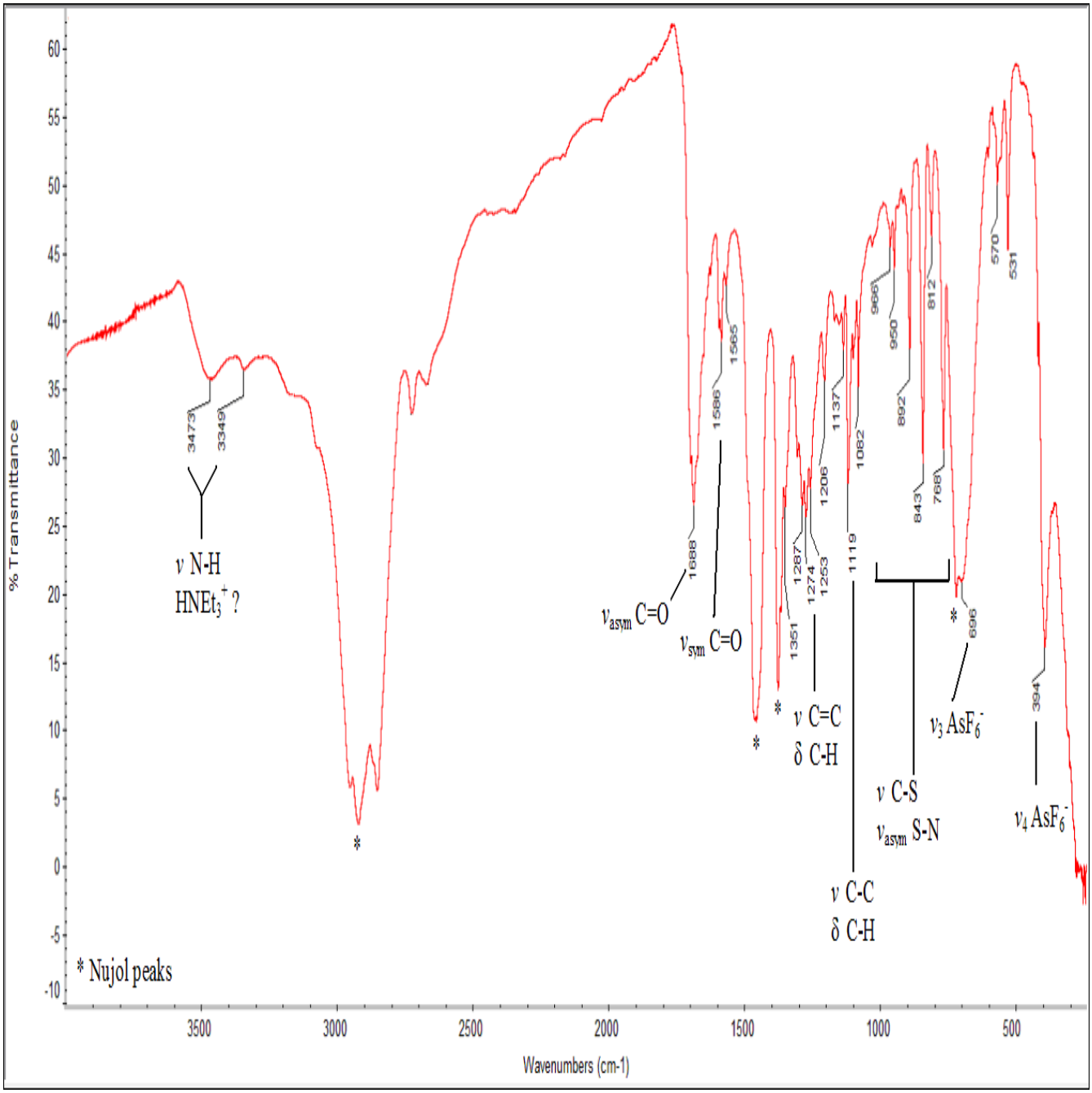

Figure S19: FT-IR of **5**AsF_6 prepared according to Equation 5 as a Nujol mull on KBr plates (32 scans, 2 cm^{-1} resolution). See Table S10 for comparison of experimental and calculated IR frequencies and tentative assignments (Note the tentative assignments: ν = stretch, δ =bending, asym. = asymmetric and sym = symmetric):

Table S10: Comparison of calculated (B3LYP/6-311++G(d,p) and experimental IR frequencies for $\mathbf{5}^{+}$ and $\mathbf{5}^{\bullet}$.

5AsF_6		Tentative Assignments [a]	$\mathbf{5}^{\bullet}$		Tentative Assignments [a]
IR/Raman (Calc.) [e]	IR (Obs.) [b]		IR/Raman (Calc.) [e]	IR (Obs.) [c]	
3202 (4/85)			3199 (1/)		
3190 (1/27)			3182 (1/)		
1698 (100/0) [d]	1688vs	ν_{asym} C=O	1659 (4/) [d]		
1691 (0/100) [d]	1586m	ν_{sym} C=O	1646 (100/) [d]	1643s, br	ν_{asym} C=O
1585 (6/31) [d]	1565w	νHC=CH	1603 (1/) [d]		
1493 (1/13)			1555 (15/)	1558vs, br	νSC=CS
1383 (3/4)	1351m,sh	Inp. νC-C + δ_{asym}C-H bending	1376 (0/)		
1269 (33/6)	1274s,br	Inp. νC-C + δ_{sym}C-H bending	1287 (20/)	1296s,br	Inp. νC-C + δ_{asym}C-H bending
				1262s,br	
1258 (2/1)			1212 (7/)	1219s,br	Inp. νC-C + δ_{sym}C-H bending
	1206w		1128 (40/)	1103m,br	δ_{sym}C-H bending
	1137w		1010 (0/)	1043m,sh	ν ring
1113 (24/19)	1119m	Inp. νC-C + δ_{sym}C-H bending	1001 (3/)	1022m,sh	Opp. δ_{asym}C-H bending
1073 (6/5)	1082w	νC-C + νC-S	922 (4/)		
1009 (0/1)	966w		880 (7/)	891w	ν ring
939 (1/0)			852 (14/)	821m,br	Opp. δ_{sym}C-H bending
930 (1/4)	950w		756 (0/)	769m,sh	δ_{asym}S-N bending
889 (1/2)	892w		702 (1/)		
866 (14/0)	843m	Opp. νC-C + δ_{sym}C-H bending	695 (1/)		
	812w		650 (1/)		
752 (11/7)	768m,sh	ν_{sym} S-N	590 (1/)		
707 (1/0)			576 (1/)		
	696vs,br	ν_3 AsF_6^-		688s,br	ν_3 AsF_6^- [e]
			551 (2/)	521w	Ring bending
689 (0/1)			492 (2/)		
595 (0/1)			446 (1/)	452w,br	Ring bending
586 (1/9)	570w		364 (0/)		
577 (0/1)			345 (7/)		
531 (7/3)	531w		313 (1/)		
436 (0/2)			245 (0/)		
427 (4/0)			198 (1/0)		
	394vs	ν_4 AsF_6^-		388s,sh	ν_4 AsF_6^- [e]
391 (1/2)			193 (1/0)		
379 (0/1)			161 (1/0)		
307 (3/1)			88 (1/0)		
250 (0/1)			72 (0/)		
186 (0/1)					
178 (1/0)					
84 (3/0)					
66 (0/1)					

[a] Assignment where made by visualization in Chemcraft [14] (ν = stretching, δ = bending, Asym. = asymmetric, Sym. = symmetric, Inp. = in-plane, Opp = out-of-plane). [b] See Figure S19 for FT-IR spectra. [c] See Figure S25 for FT-IR spectra [d] The ν C=O and ν (OC)-C=C-(CO) stretching frequencies are scaled by 0.965. [e] Calculated at the B3LYP/6-311++G(d,p) level of theory.

1.4.9 Multinuclear NMR of $5AsF_6$ prepared according to Equation 5 in liquid SO_2

SO_2 (4.717 g) was condensed onto **5**AsF_6 (0.138 g, 0.37 mmol) in a 10 mm NMR tube (Figure S1d) and flame sealed. Upon warming a dark orange solution over a small quantity of an unidentified brown insoluble was obtained. See Figure S20-S23 for actual multinuclear NMR spectra.

^{1}H-NMR: The ^{1}H-NMR (Figure S20) was assigned to $\mathbf{5}^+$ (broad resonance δ 8.43 (C-H)) and $HNEt_3^+$ (δ 6.34 (N-H), δ 4.33 (N-C***H***$_2$CH$_3$) and δ 2.40 (N-CH$_2$C***H***$_3$)). The integration in Figure S20 is consistent with Equation 5 (e.g. approximately one $\mathbf{5}^+$ relative to two $HNEt_3^+$).

^{13}C-NMR: The decoupled ^{13}C-NMR (Figure S21b) was consistent with $\mathbf{5}^+$ (δ 177.2 (C-S), δ 175.1 (C=O) and δ 140.0 (C-H; $J_{C\text{-}H}$ = 177 Hz from coupled ^{13}C-NMR (Figure S21a)) and $HNEt_3^+$ (δ 49.0 (N-***C***H$_2$CH$_3$) and δ (N-CH$_2$***C***H$_3$), respectively in Figure S21.

^{14}N-NMR: The ^{14}N-NMR (Figure S22) exhibited 9 resonances. A broad resonance at δ 1.8 ($\nu_{1/2}$ 662 Hz) is assigned to $\mathbf{5}^+$ (c.f. δ -7.4 ($\nu_{1/2}$ 540 Hz) for $\mathbf{1}^+$), while a doublet centered at δ -317.5 ($\nu_{1/2}$ 109 Hz, $J_{N\text{-}H}$ = 50 Hz) and a poorly resolved pentet centered at δ -360.0 ($\nu_{1/2}$ 139 Hz, $J_{N\text{-}H}$ = 54 Hz) are assigned to $HNEt_3^+$ and NH_4^+, respectively (Figure S22). Six other sharp resonances δ -69.7, -113.3, -133.4, -140.5, -169.9, - 190.1 are unassigned which based on the integration are ~11% of the total species in solution.

^{19}F-NMR: The ^{19}F-NMR (Figure S23) shows three resonances. Two are assigned to AsF_3 (δ -41.4) and AsF_6^- (Expected 1:1:1:1 quartet appears exchange broadened as a 1:1 doublet centered at δ -56.3) while one δ -46.1 is unassigned (Figure S23). The integration ratio of AsF_3 and AsF_6^- only is 1:9, respectively. This corresponds to ~ 25 % AsF_3 according to Equation 5 remains in isolated **5**AsF_6 after removal of the volatiles (Section 1.4.4).

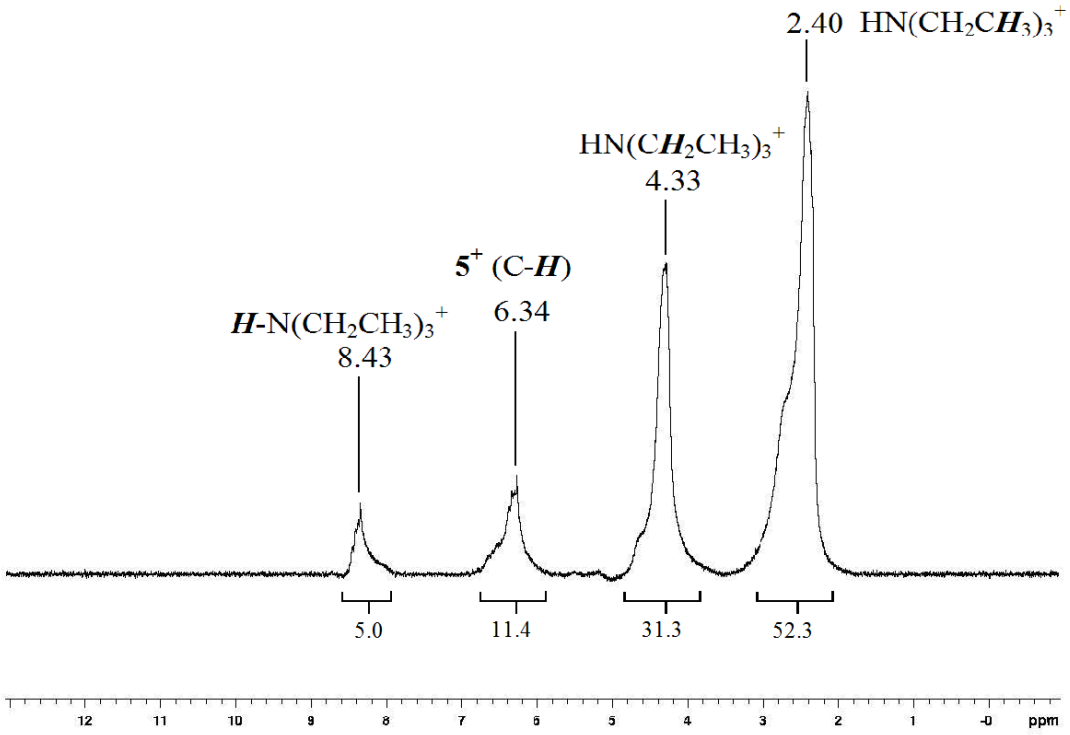

Figure S20: ^{1}H-NMR of **5**AsF_6 prepared according to Equation 5 in liquid SO_2 at 25 ^{o}C.

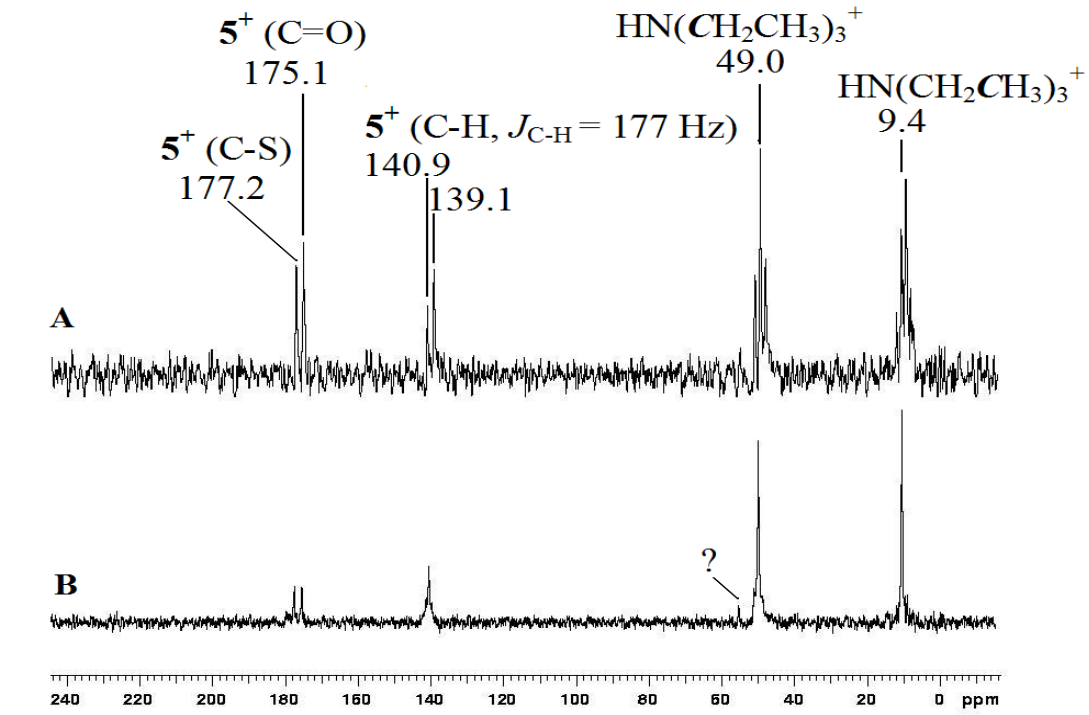

Figure S21: ^{13}C-NMR of **5**AsF_6 prepared according to Equation 5 in liquid SO_2 at 25 ^{o}C where a) coupled to establish C-H assignment and b) is decoupled.

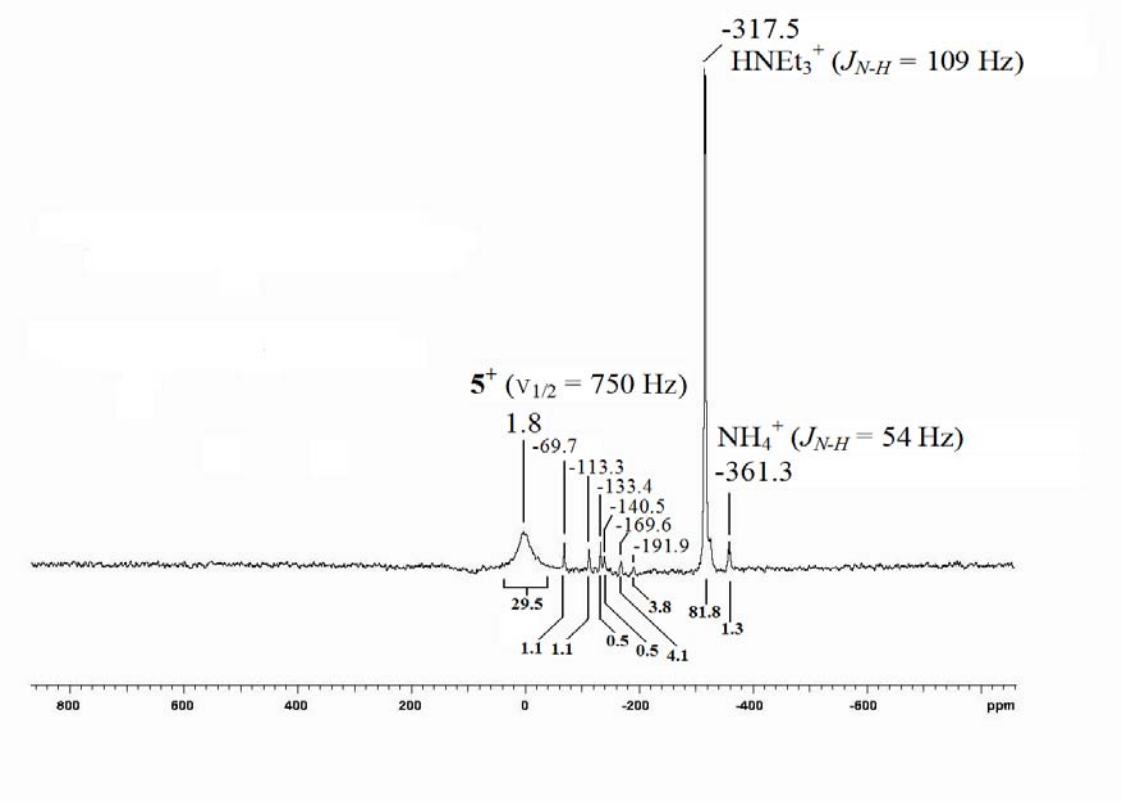

Figure S22: ^{14}N-NMR of **5**AsF_6 prepared according to Equation 5 in liquid SO_2 at 25 ^{o}C.

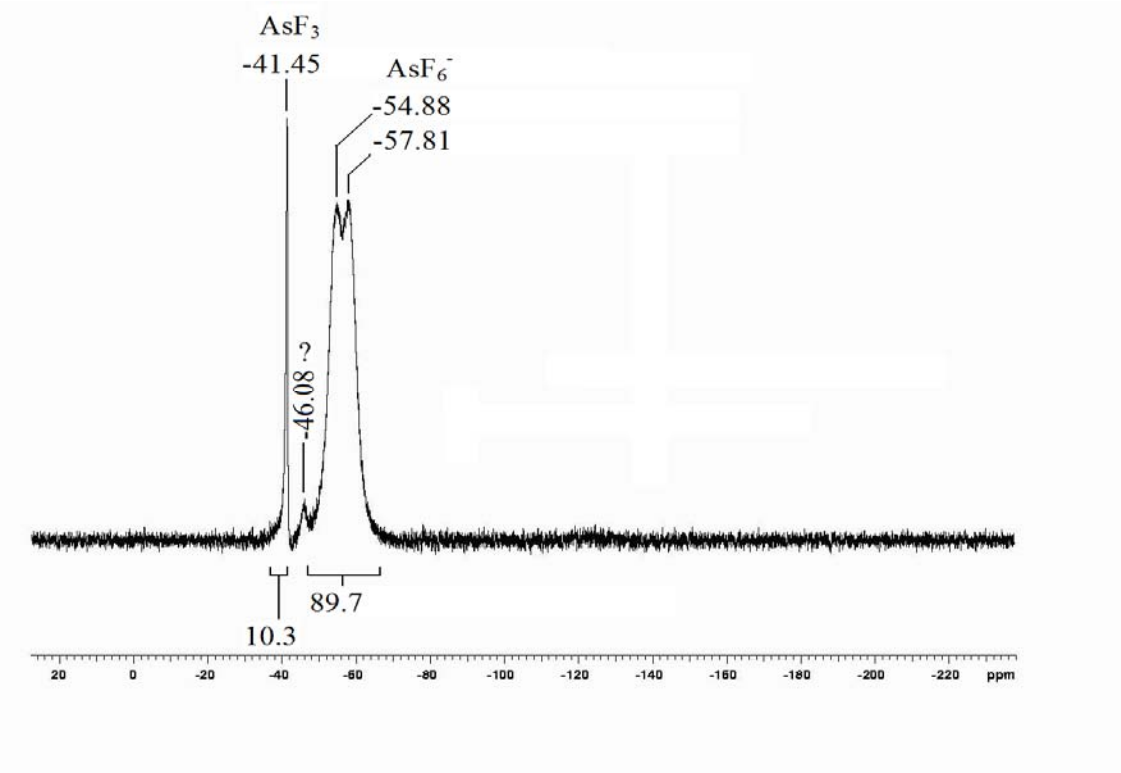

Figure S23: ^{19}F-NMR of **5**AsF_6 prepared according to Equation 5 in liquid SO_2 at 25 ^{o}C.

1.4.10 *In situ* reduction of $5AsF_6$ prepared according to Equation 5 with ferrocene (Cp_2Fe) in CH_2Cl_2 and toluene according to Equation 9

5AsF_6 (0.020 g, 0.054 mmol) and Cp_2Fe (0.012 g, 0.065 mmol) were added to bulb A of a vessel of Type B (10 ml bulbs, Figure S1b) incorporating a 3 mm EPR tube directly attached via a 1⁄4 inch Pyrex tube. CH_2Cl_2 (2.482 g; ~ 2 ml) and Toluene-d^8 (0.912 g; ~ 1 ml) where consecutively condensed into bulb A. Upon warming the solution to ambient temperature a pale yellow solution over a blue-grey solid (containing $CpFeAsF_6$) was obtained. The solution was filtered into the EPR tube. The EPR consisted of a 1:1:1 triplet (Obs. a_N = 1.011 mT; Calc. a_N = 1.063 mT; See Figure 2b in main text of Chemical Communication and Table S6 for a comparison of experimental and calculated hyperfine coupling constants) which was very weak (very high gain needed) and is similar with **2**$^\bullet$ (c.f. 1.089 mT)[15] and related 1,3,2-dithiazolyl radicals.[21] Modulation amplitude 0.2 mT, spectral width 5 mT, sweep time 60s, gain $9x10^2$.

1.4.11 Reduction of $5AsF_6$ prepared according to Equation 5 with ferrocene (Cp_2Fe) in CH_2Cl_2 according to Equation 9

5AsF_6 (0.378 g, 1.01 mmol) and Cp_2Fe (0.183 g, 0.98 mmol) were loaded in to bulb A of a vessel of Type B (10 ml bulbs, Figure S1b) incorporating a 3 mm ESR tube directly attached by a 1⁄4 inch Pyrex tube. CH_2Cl_2 (6.688 g; ~ 5 ml) was condensed into bulb A. A pale blue solution over a purple-brown solid was obtained upon warming to ambient temperature. The solution was stirred for 2 hrs and the more soluble fraction filtered to bulb B. The ESR of this more soluble fraction was a very weak 1:1:1 triplet (Figure S24). The volatiles were condensed back to bulb A and the more soluble fraction washed to bulb B. This was repeated several times. The volatiles were removed under dynamic vacuum and SO_2 (4.139 g) condensed into bulb A. The more soluble blue-green (c.f. Cp_2FeAsF_6) solution over the purple-brown insoluble was filtered to bulb B. The volatiles were condensed back to bulb A. The purple-brown solid was washed until the filtrate was colorless (3 times total). The volatiles were removed under dynamic vacuum. The purple brown insoluble in bulb A (0.147 g, 0.80 mmol and 79 % yield of **5**$^\bullet$ based on **5**(AsF_6) and Equation 9) and the blue solid (c.f. Cp_2FeAsF_6) in bulb B (0.398 g) were collected in the drybox. The IR of the purple-brown solid in bulb A was obtained as a Nujol mull on KBr plates and was consistent with **5**$^\bullet$ (Figure S25) on comparison of the experimental and calculated IR given in Table S7. We note the assigned ν C=O of **5**$^\bullet$ is at 1643 cm^{-1} (c.f. ν C=O of **5**$^+$ is 1688 cm^{-1}). The tentative assignment of 688 and 388 cm^{-1} to ν_3 AsF_6^- and ν_4 AsF_6^-, respectively are attributed to the presence of Cp_2FeAsF_6.

Equation 9:

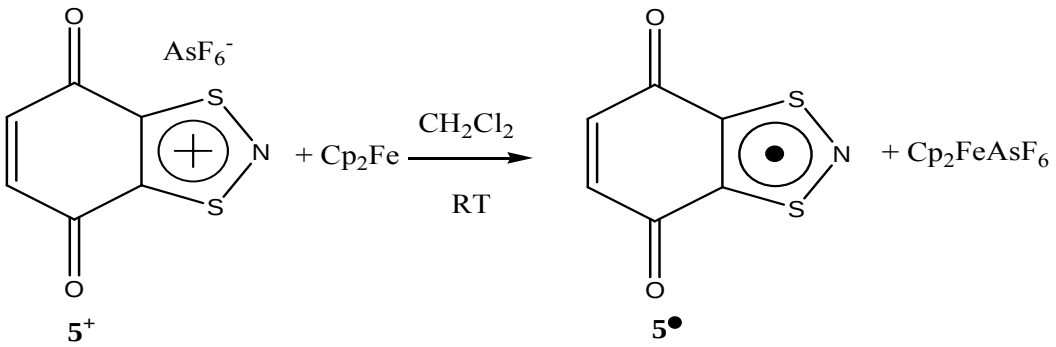

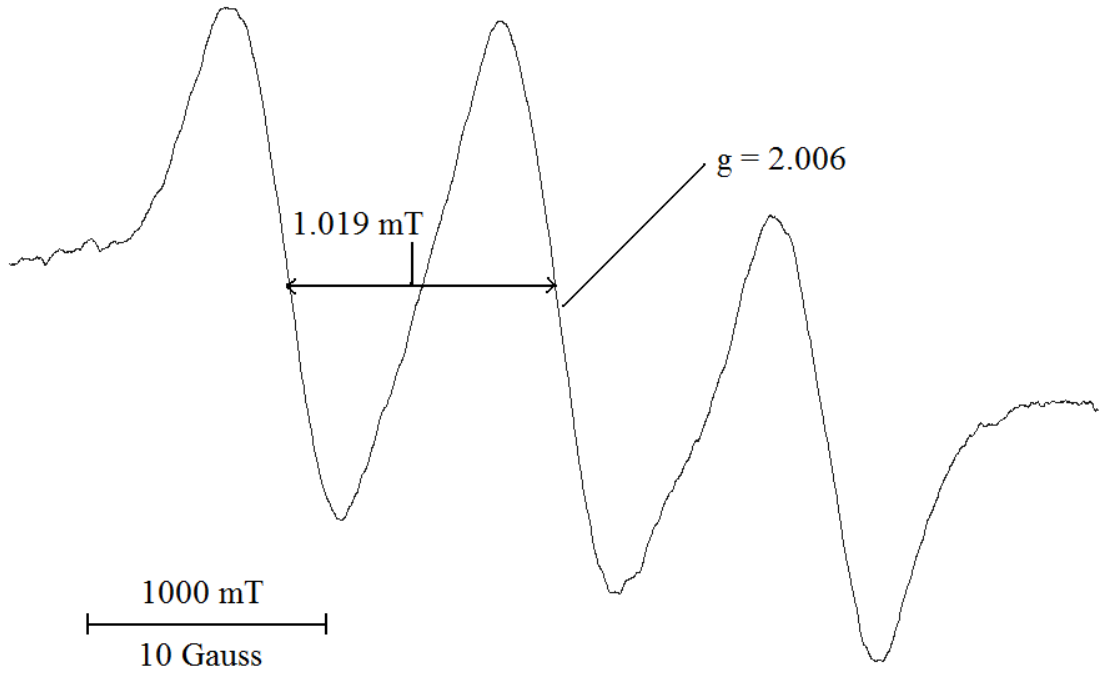

Figure S24: The X-band EPR of **5**$^{\bullet}$ prepared according to Equation 9 in CH_2Cl_2 at 25 ^{o}C (Sweep width 5 mT, Sweep time 90 s, Modulation amplitude 0.4 mT, gain $9*10^2$)

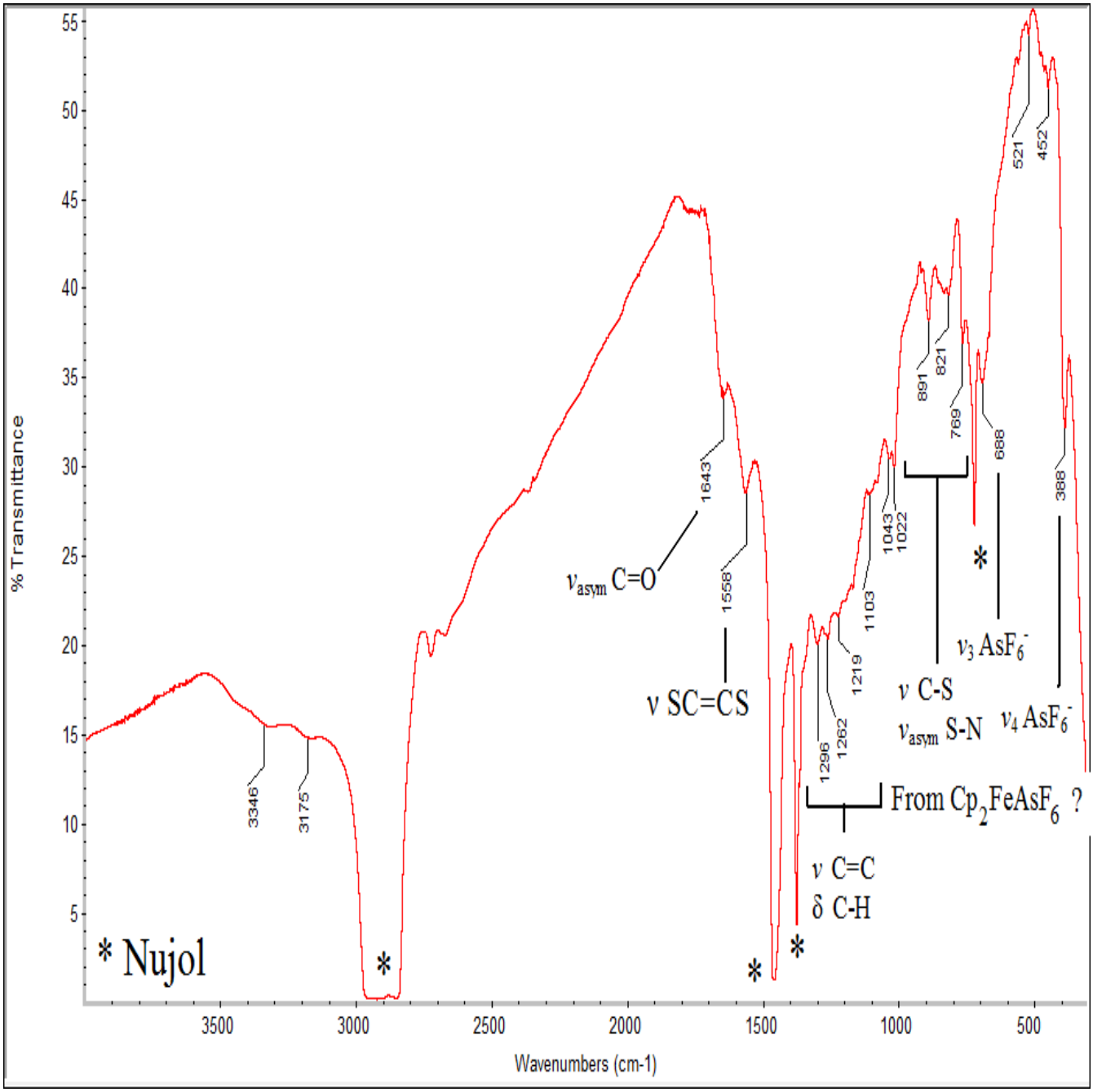

Figure S25: The FT-IR of **5**$^{\bullet}$ prepared according to Equation 9 as a Nujol mull on KBr (32 scans, 2 cm^{-1} resolution). See Table S10 for comparison of experimental and calculated IR frequencies and tentative assignments (Note the tentative assignments: ν = stretch, δ =bending, asym. = asymmetric and sym = symmetric):

1.4.12 Reaction of 5AsF$_6$ with excess SNSAsF$_6$ in SO$_2$ leading to 3(AsF$_6$)$_2$ according to Equation 2-4 in Scheme 1

5AsF$_6$ (0.809 g, 2.17 mmol, see Section 1.4.8) and SNSAsF$_6$ (1.029 g, 3.85 mmol) were added to bulb A of a vessel of Type B (Figure S1b). SO$_2$ (15.347 g) was condensed onto the solid and a blue solution was obtained on warming to ambient temperature. The solution was stirred for 5 days. After 5 days a beige-white insoluble under a blue solution

was obtained. The more soluble fraction was filtered to bulb B. The volatiles were condensed back to bulb A. The more soluble fraction was filtered to bulb B. This was repeated (x 3) until the more soluble fraction over the beige-white insoluble in bulb A were clear and colorless. The volatiles were removed under dynamic vacuum and the beige white solid in bulb A was collected (1.428 g, 85 % yield of **3**$(AsF_6)_2$ based on **5**AsF_6 and Equation 9) in the drybox. The IR of the beige-white solid in bulb A was obtained as a Nujol mull on KBr plates (Figure S26a) but was poorly resolved which suggested a possible mixture of **5**(AsF_6) and **3**$(AsF_6)_2$ by comparison to Figure S19 (**5**AsF_6) and Figure S9 (**3**$(SbF_6)_2$). See also the comparison of experimental and calculated IR frequencies given in Table S4.
The ^{13}C-NMR (CD_3CN, 25 ^{o}C) of the beige-white solid from bulb A in a 10 mm Pyrex NMR tube indicate the presence of only two resonances, δ -178.6 and δ 156.0 assigned to C=O and C-S of $\mathbf{3}^{2+}$ respectively (Figure S27). The calculated and experimental ^{13}C-NMR of $\mathbf{3}^{2+}$ are compared with related 1,3,2-dithiazolyls in Table S2.

Overall summary of Equation 3-4 in Scheme 1:

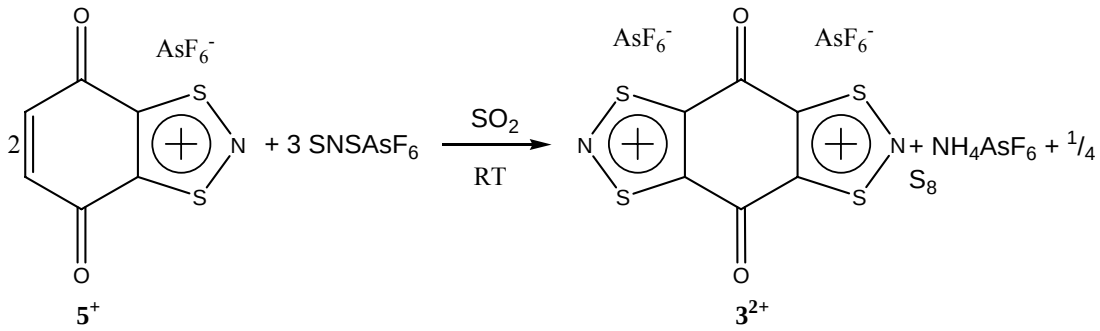

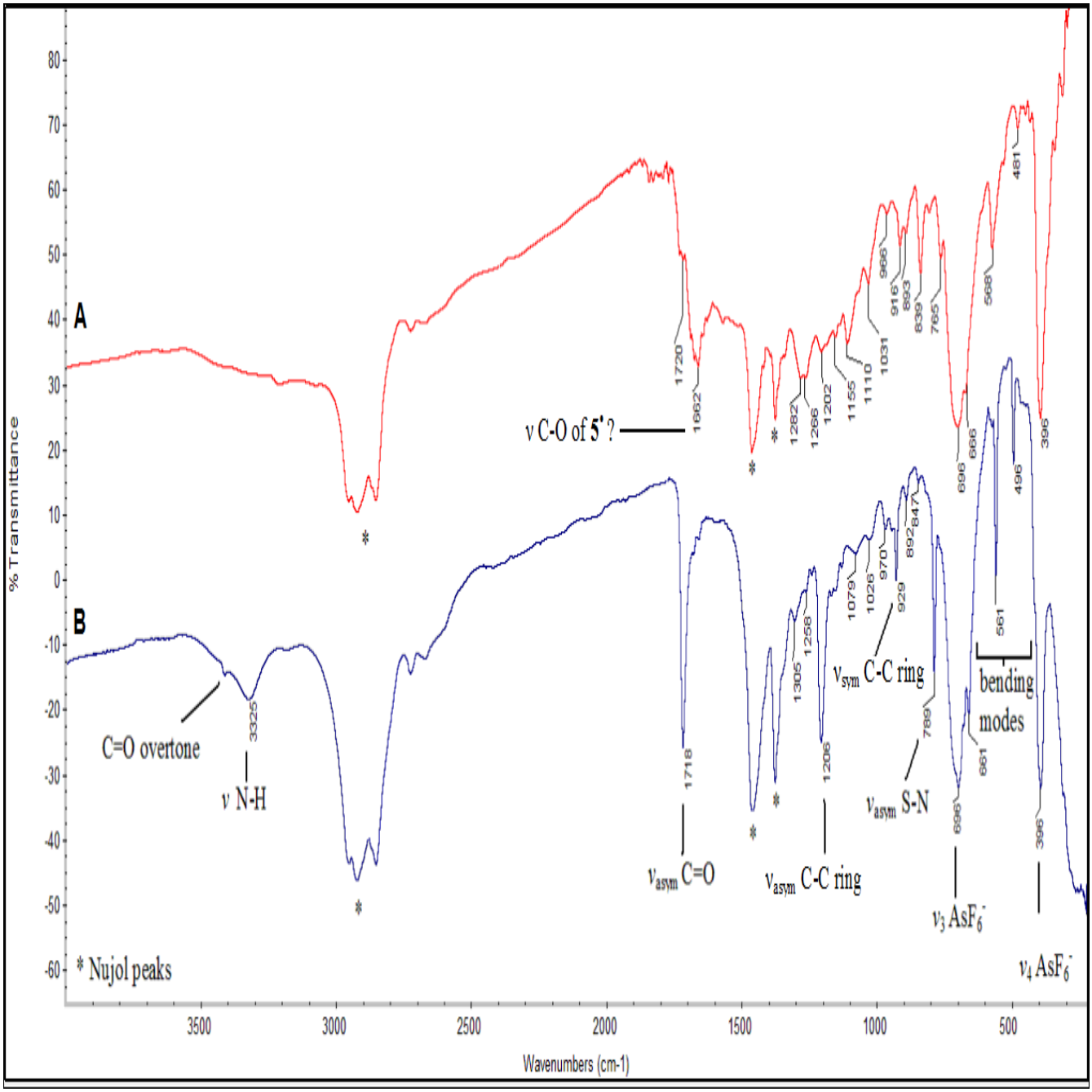

Figure S26: FT-IR of a) crude **3**$(AsF_6)_2$ prepared according to Equation 3-4 in Scheme 1 and b) purified **3**$(AsF_6)_2$ (Section 1.4.13, below) as Nujol mull on KBr plates (32 scans, 2 cm^{-1} resolution). See Table S4 for comparison of experimental and calculated IR frequencies and tentative assignments (Note the tentative assignments: ν = stretch, δ =bending, asym. = asymmetric and sym = symmetric):

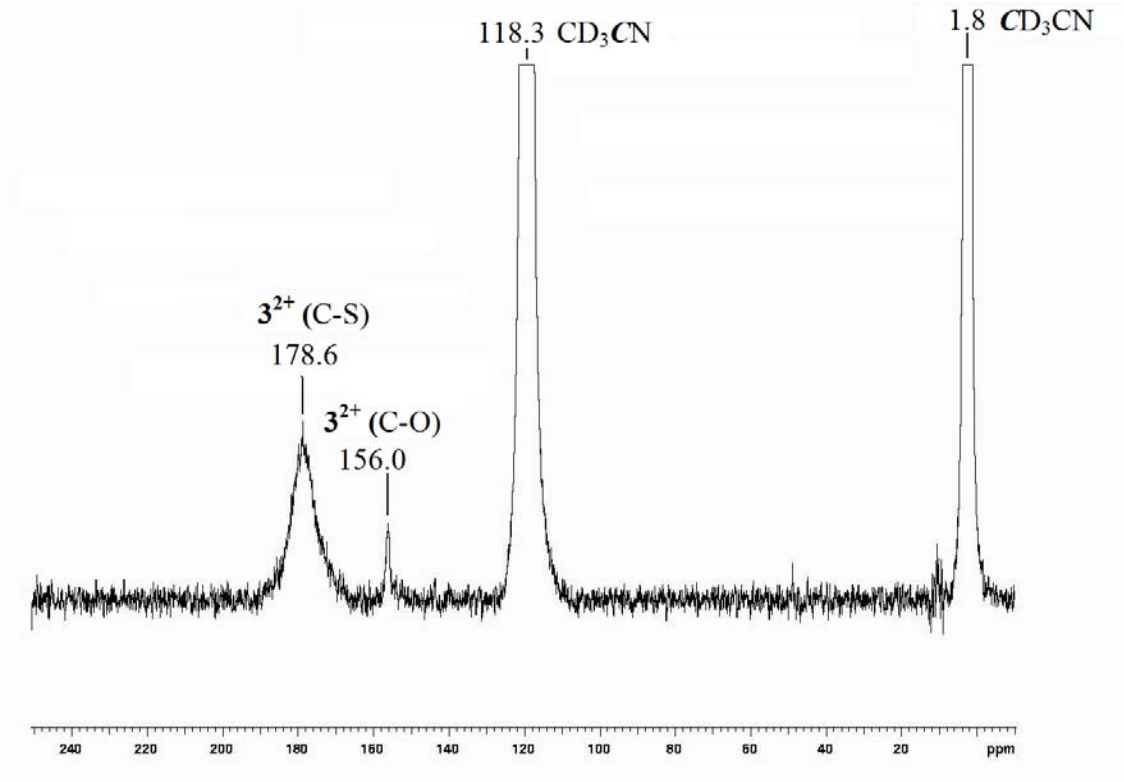

Figure S27: The ^{13}C-NMR (CD_3CN, 25 ^{o}C) of **3**$(AsF_6)_2$ prepared according to Equation 3-4 in Scheme 1

1.4.13 Purification of 3$(AsF_6)_2$ prepared according to Equation 3-4 in Scheme 1 from CH_3CN and CH_2Cl_2

Crude **3**$(AsF_6)_2$ (1.398 g) was added to bulb A of a vessel of Type B (Figure S1b). CH_3CN (8.671 g; ~ 11 ml) was condensed into bulb A. A red solution was obtained on warming to ambient temperature over a beige-white insoluble. The red solution quickly turned green-blue upon stirring for 5 minutes. The more soluble fraction was filtered to the bulb B and the volatiles condensed back into bulb A. The more soluble fraction was filtered to bulb B. This was repeated 3 more times. CH_2Cl_2 (27.036 g; ~ 20 ml) was condensed into bulb B. Upon warming a green solution over clear colorless crystals were obtained. The more soluble fraction in bulb B was filtered into bulb A. A small volume (~ 2 ml) of the volatiles was condensed back to bulb B. The more soluble fraction was filtered to bulb A. This was repeated twice more. The volatiles were removed under dynamic vacuum. The clear colorless crystals in bulb B (0.812 g, 1.27 mmol, 68 % yield of **3**$(AsF_6)_2$ based on **5**AsF_6 and Equation 8) and the solid in bulb A (0.543 g) were collected in the drybox. The IR of the clear and colorless crystals in bulb B was obtained as a Nujol mull on CsI plates (Figure S26b) and was consistent with **3**$(AsF_6)_2$ by comparison of the experimental and calculated IR frequencies given in Table S4. The X-ray crystal structure was determined (Figure S28) and the calculated and experimental bond lengths (Å) and angles (^{o}) are compared in Table S3.

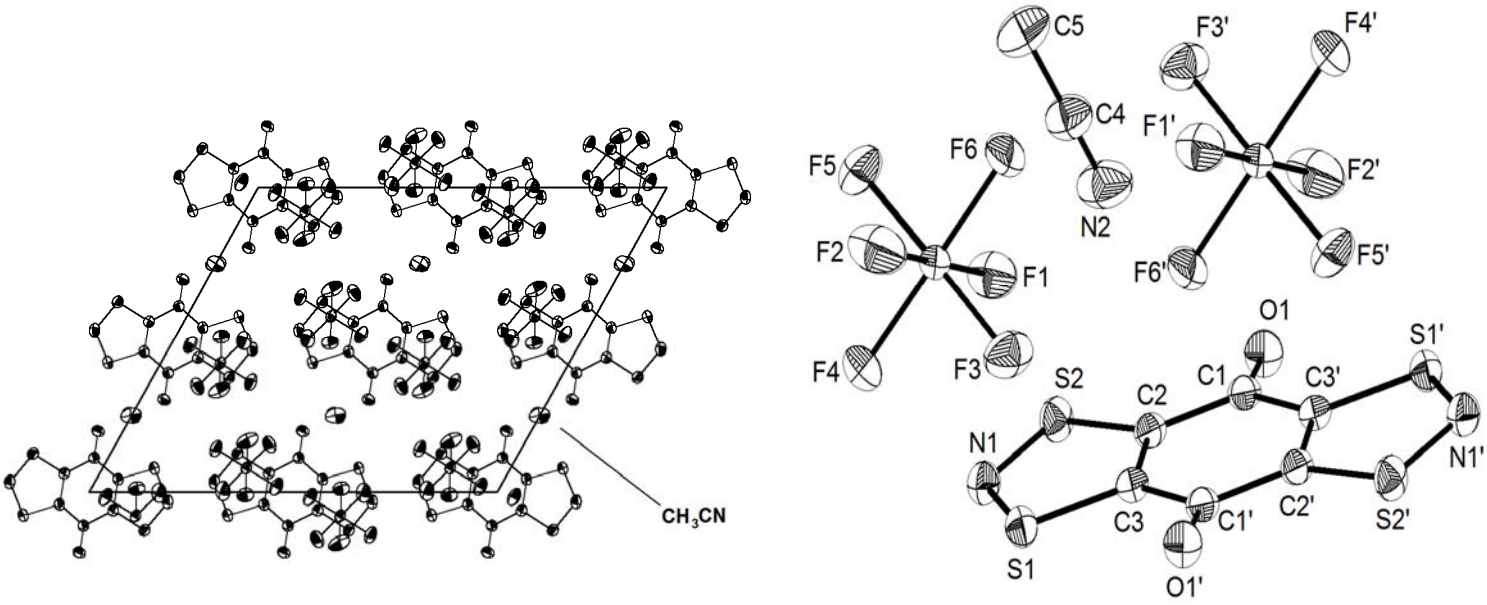

Figure S28: The X-ray crystal structure of **3**$(AsF_6)_2$•CH_3CN where a) a view of the unit cell along the b-axis and b) the atom labelling within the asymmetric unit. Thermal ellipsoids are given at 50 % probability. A comparison of experimental and calculated bond distances (Å) and angles (^{o}) are given in Table S3.

References:

1 D.R. Aris, C.Knapp, J. Passmore, and X. Wang, *J. Flourine Chem.,* 2005, **126**, 1368.
2 (a) M. Murchie and J. Passmore, *Inorg. Synth.* 1988, **27**, 76. (b) M.P. Murchie, R. Kapoor, J. Passmore, and G. Schatte, T. Way, *Inorg. Synth.* 1997, **31**, 102.
3 H.E. Gottlieb, V. Kotlyer, and A. Nudelman, *J. Org. Chem.,* 1997, **62**,7512.
4 M.J. Frisch, G.W. Trucks, H.B. Schlegel, G.E. Scuseria, M.A. Robb, J.R. Cheeseman, J.A. Montgomery Jr., T. Vreven, K. N. Kudin, J. C. Burant, J. M. Millam, S. S. Iyengar, J. Tomasi, V. Barone, B. Mennucci, M. Cossi, G. Scalmani, N. Rega, G. A. Petersson, H. Nakatsuji, M. Hada, M. Ehara, K. Toyota, R. Fukuda, J. Hasegawa, M. Ishida, T. Nakajima, Y. Honda, O. Kitao, H. Nakai, M. Klene, X. Li, J. E. Knox, H. P. Hratchian, J. B. Cross, V. Bakken, C. Adamo, J. Jaramillo, R. Gomperts, R. E. Stratmann, O. Yazyev, A. J. Austin, R. Cammi, C. Pomelli, J. W. Ochterski, P. Y. Ayala, K. Morokuma, G. A. Voth, P. Salvador, J. J. Dannenberg, V. G. Zakrzewski, S. Dapprich, A. D. Daniels, M. C. Strain, O. Farkas, D. K. Malick, A. D. Rabuck, K. Raghavachari, J. B. Foresman, J. V. Ortiz, Q. Cui, A. G. Baboul, S. Clifford, J. Cioslowski, B. B. Stefanov, G. Liu, A. Liashenko, P. Piskorz, I. Komaromi, R. L. Martin, D. J. Fox, T. Keith, M. A. Al-Laham, C. Y. Peng, A. Nanayakkara, M. Challacombe, P. M. W. Gill, B. Johnson, W. Chen, M.W. Wong, C. Gonzalez, and J. A. Pople, GAUSSIAN 03, Revision C. 02, Gaussian, Inc., Wallingford, CT, 2004.
5 S. Brownridge, J. Passmore, X. Sun, Can. J. Chem. 1998, **76**, 1220.
6 A. Decken, H.D.B. Jenkins, A. Mailman, J. Passmore and K.V. Shuvaev, *Inorg. Chim. Acta,* 2008, **361**, 521.
7 a) A.D. Becke, *J. Chem. Phys.,* 1993, **98**, 1372. b) C. Lee, W. Yang, and R.G. Parr, *Phys. Rev. B,* 1988, **37**, 785. c) P. J. Stevens., F. J .Devlin, C.F. Chablowski and M. J. Frisch, *J. Phys. Chem.,* 1994, **98**, 11623.
8 (a) R. Krishnan, J.S. Binkley, R. Seeger and J. Pople, *J. Chem. Phys.*, 1980, **72** 650. b) T. Clark, J. Chandrasekhar, P. v. R. Schleyer, *J. Comp. Chem.,* 1983, **4**, 294.
9 (a) C. Adamo, V. Barone, *J. Chem. Phys.,* 1998, **108**, 664. (b) E. Cances, B. Mennucci, J. Tomasi, *J. Chem. Phys.,* 1997, **107**, 3032. (c) M. Cossi, V. Barone, B. Mennucci, J. Tomasi, *Chem. Phys. Lett.,* 1998, **286**, 253.
10 (a) J.P. Perdew, K. Burke, M. Ernserhof, *Phys. Rev. Lett.,* 1997, **78**, 1396. (b) J.P. Perdew, M. Ernserhof,
K. Burke, *J. Chem. Phys.*, 1996, **105**, 9982. (c) C. Adamo, V. Barone, *J. Chem. Phys.,* 1999, **110**, 6158.
11 C. Adamo, V. Barone, *Chem. Phys. Lett.,* 1997, **274**, 242.
12 V. Barone, in: D.P. Chong (Ed.), *Recent Advances in Density Functional Methods, Part I,* World Scientific, Singapore, 1996.
13 M. J. Frisch, G. W. Trucks, H. B. Schlegel, G. E. Scuseria, M. A. Robb, J. R. Cheeseman, V. G. Zakrzewski, J. A. Montgomery Jr., R. E. Stratmann, J. C. Burant, S. Dapprich, J. M. Millam, A. D. Daniels, K. N. Kudin, M. C. Strain, O. Farkas, J. Tomasi, V. Barone, M. Cossi, R. Cammi, B. Mennucci, C. Pomelli, C. Adamo, S. Clifford, J. Ochterski, G. A. Petersson, P. Y. Ayala, Q. Cui, K. Morokuma, D.K. Malick, A. D. Rabuck, K. Raghavachari, J. B. Foresman, J. Cioslowski, J. V. Ortiz, B. B. Stefanov, G. Liu, A. Liashenko, P.Piskorz, I. Komaromi, R. Gomperts, R. L. Martin, D. J. Fox, T. Keith, M. A. Al-Laham, C. Y. Peng, A. Nanayakkara, C. Gonzalez, M. Challacombe, P. M. W. Gill, B. G. Johnson, W. Chen, M. W. Wong, J. L. Andres, M. Head-Gordon, E. S. Replogle, J. A. Pople, *Gaussian 98*, revision A.7, Gaussian, Inc.: Pittsburgh, PA, 1998.
14 D. A. Zhurko, G. A. Zhurko, *ChemCraft 1.5*; Plimus: San Diego, CA, 92130; http://www.chemcraftprog.com (accessed Dec 2006).
15 A. Decken, A. Mailman, S. Mattar and J. Passmore, *Chem. Commun.,* 2005, 2366.
16 X. Zhao, H. Imahori, C.G. Zhan, Y. Sakata, S. Iwata and T. Kitagawa, *J. Phys. Chem. A,* 1997, **101**, 622.
17 J. Passmore and M.J. Schriver, *Inorg. Chem.,* 1988, **27**, 2749.
18 a) K. Terago, J. Olah, J.M.L. Martin, T. Veszpremi, C. van Alsenoy and F. Blockhuys, *Chem. Phys. Lett.,* 2005, **413**, 440. b) J. van Droogenbroeck, K. Tersago, C. van Alsenoy and F. Blockhuys, *Chem. Phys. Lett.,* 2004, 399, 516. c) J. van Droogenbroeck, K. Tersago, C. van Alsenoy, S.M. Aucott, H.L. Hutton, J.D. Woollins and F. Blockhuys, *Eur. J. Inorg. Chem.,* 2004, 3798.
19 a) G. MacLean, *Ph. D. Thesis*, University of New Brunswick, 1986. b) J. Passmore,
20 T.S. Cameron, A. Mailman, J. Passmore and K.V. Shuvaev, *Inorg. Chem.*, 2005, **44**, 6524.
21 a) J.M. Rawson, A. Alberola and A. Whalley, *J. Mater. Chem.,* 2006, **16**, 2560. b) J.M. Rawson and G.D. McManus, *Coord. Chem. Rev.,* 1999, **189**, 135.
22 a) K.A. Williams, M.J. Nowak, E. Dormann and F. Wudl, *Synth. Met.,* 1986, **14**, 233. b) G. Wolmershauser, M. Schnauber, T. Wilhelm and L.H. Sutcliffe, *Synth. Met.,* 1986, **14**, 239. c) E. Dormann, M.J. Nowak, K.A. Williams, R.O. Angus Jr., and F. Wudl, *J. Am. Chem. Soc.,* 1987, **109**, 2594.
23 E.G. Awere, N. Burford, R.C. Haddon, S. Parsons, J. Passmore, J.V. Waszczak and P.S. White, *J. Chem. Soc., Dalton Trans.,* 1990, 4281.

24 W.V.F. Brooks, S. Brownridge, J. Passmore, M.J. Schriver and X. Sun, *J. Chem. Soc., Dalton Trans.,* 1996, 1997.
25 J. Trotter, Acta Cryst. 1960, **13**, 86.